ALBA-SSRF Bilateral Workshop
December 16-18, 2013

Current Status of SSRF

Jianhua He and Zhentang Zhao
Shanghai Synchrotron Radiation Facility
Shanghai Institute of Applied Physics, CAS, China

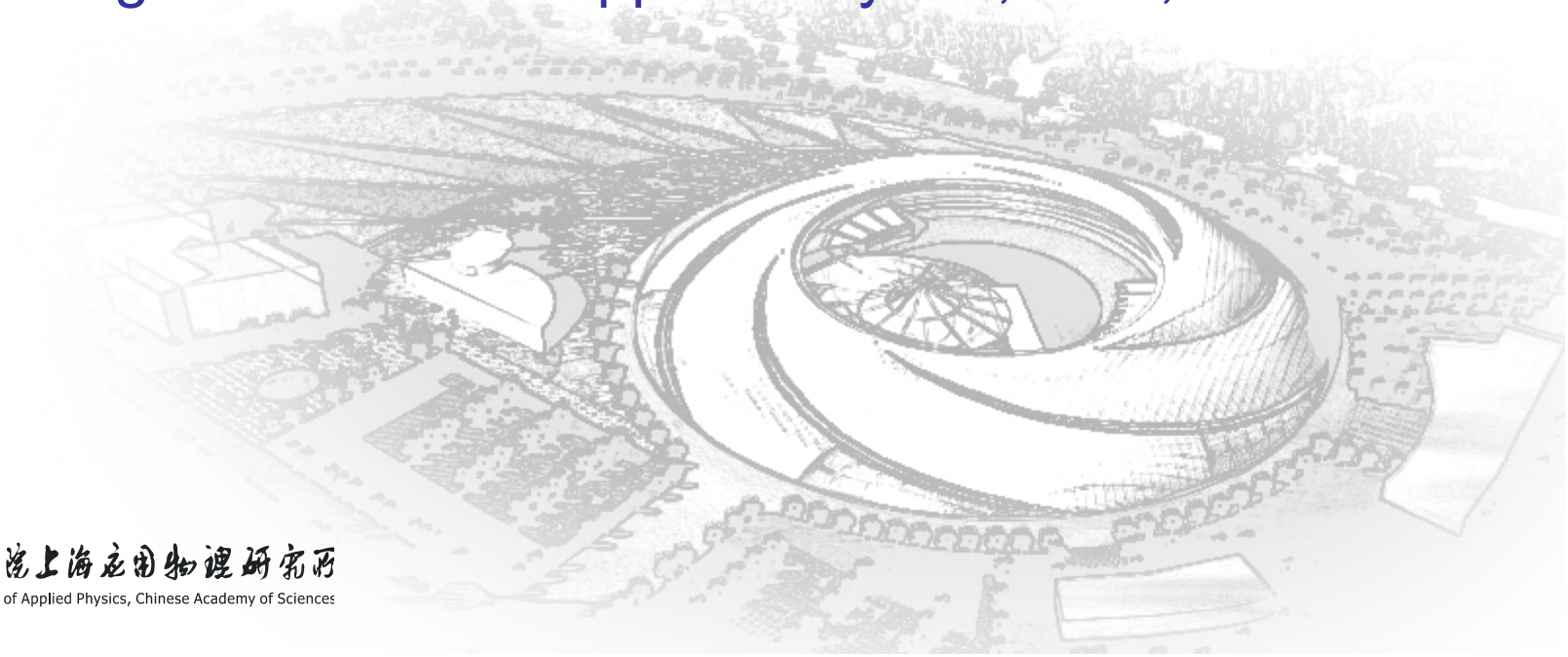

SINAP 中国科学院上海应用物理研究所
Shanghai Institute of Applied Physics, Chinese Academy of Sciences

Outline

- Overview of SSRF
- The Status of SSRF Operation
- Highlights of User Experiments
- Ongoing Projects at SSRF
- Future Programs

Overview of Shanghai Synchrotron Radiation Facility

- SSRF is an intermediate energy 3rd generation light source jointly funded by Chinese Academy of Sciences (CAS), Shanghai Municipal Government and the central government of China;

- Major scientific fields(at present)
  - Biological Sciences
  - Physical and Materials Sciences
  - Chemical and Environmental Sciences
  - Bio-medical, Energy and Industrial Applications

The SSRF Complex: Phase-I Project

7 Phase-I Beamlines

Storage Ring
3.5GeV, C=432m

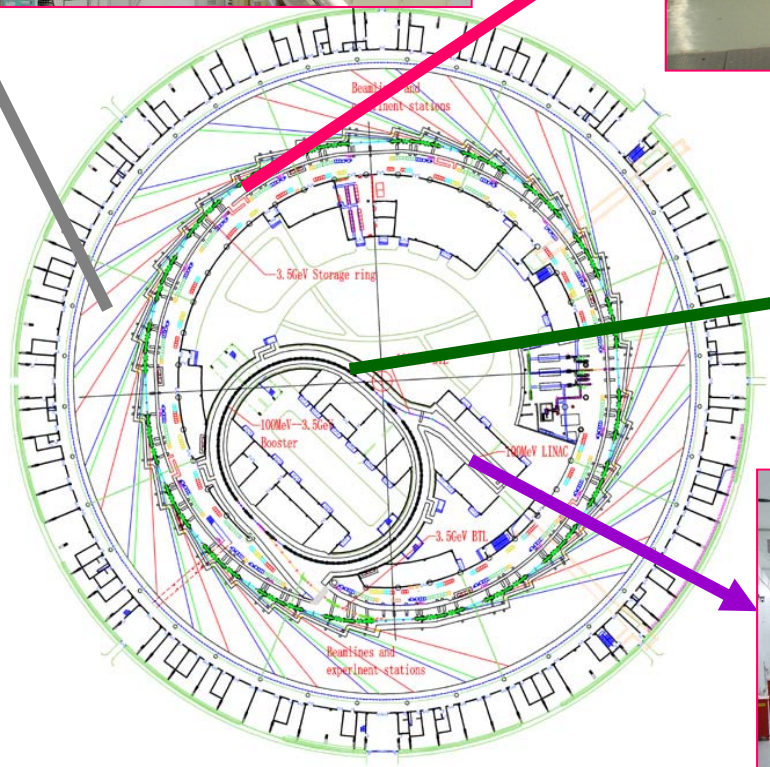

Booster
3.5GeV, C=180m

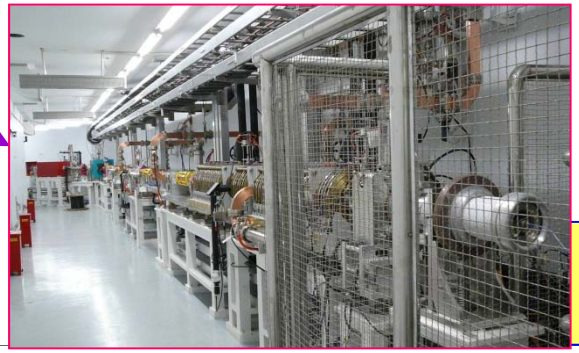

Electron Linac
150MeV

Main Parameters of Storage Ring

- Storage Ring Energy: 3.5 GeV
- Circumference: 432 m
- Natural Emittance: 3.9 nm-rad (2.9 achieved now)
- Beam Current: 200 ~ 300 mA
- Beam Lifetime: ~20 hrs (Top-up injection since December 2012)
- Straight Sections: 4×12.0 m, 16×6.5 m
- RF Voltage: 4.0~6.0 MV
- Max. Beam Power: ~600kW

SSRF provides very bright photon beams from 0.1-20keV

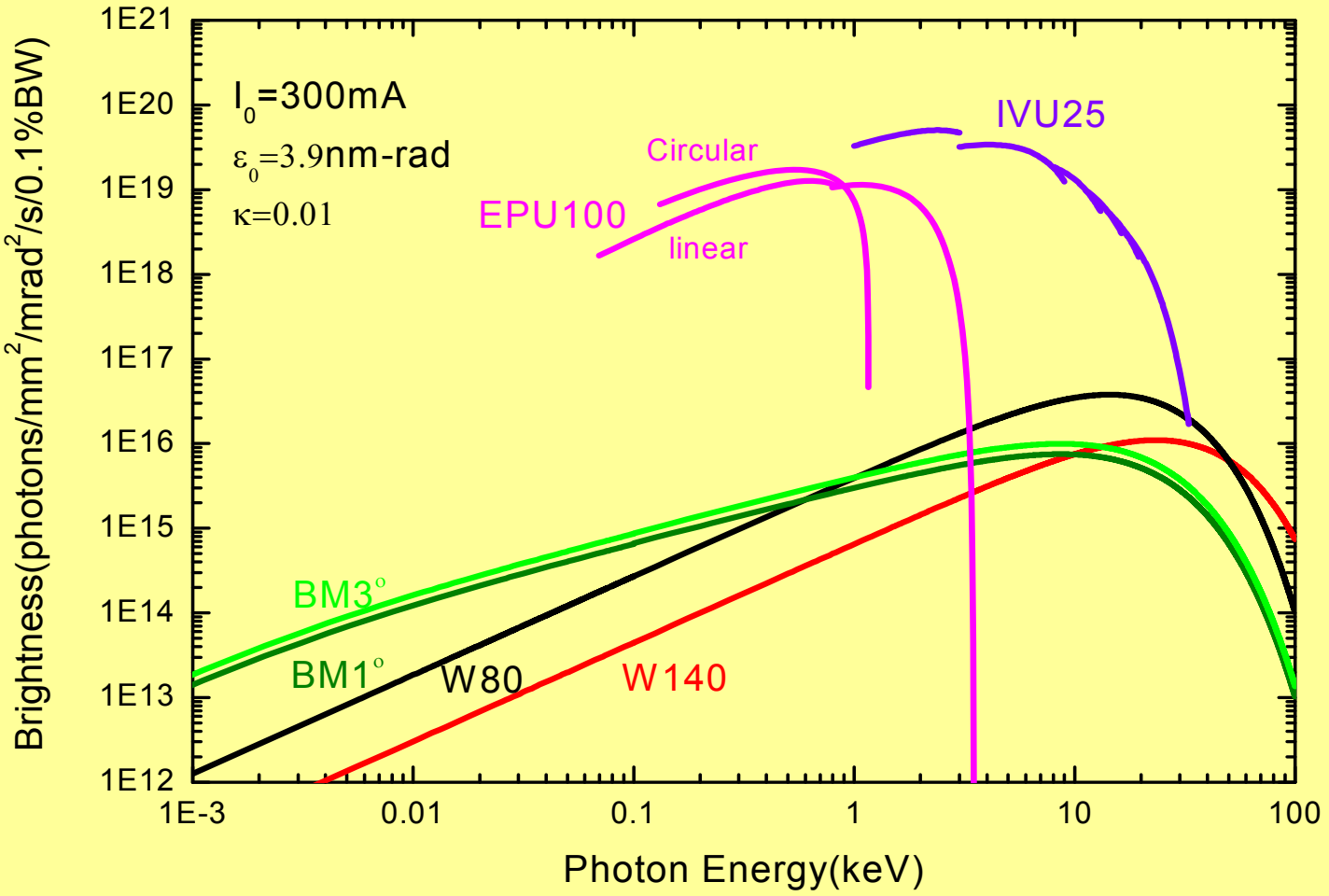

SSRF provides high flux photon beams up to 50keV

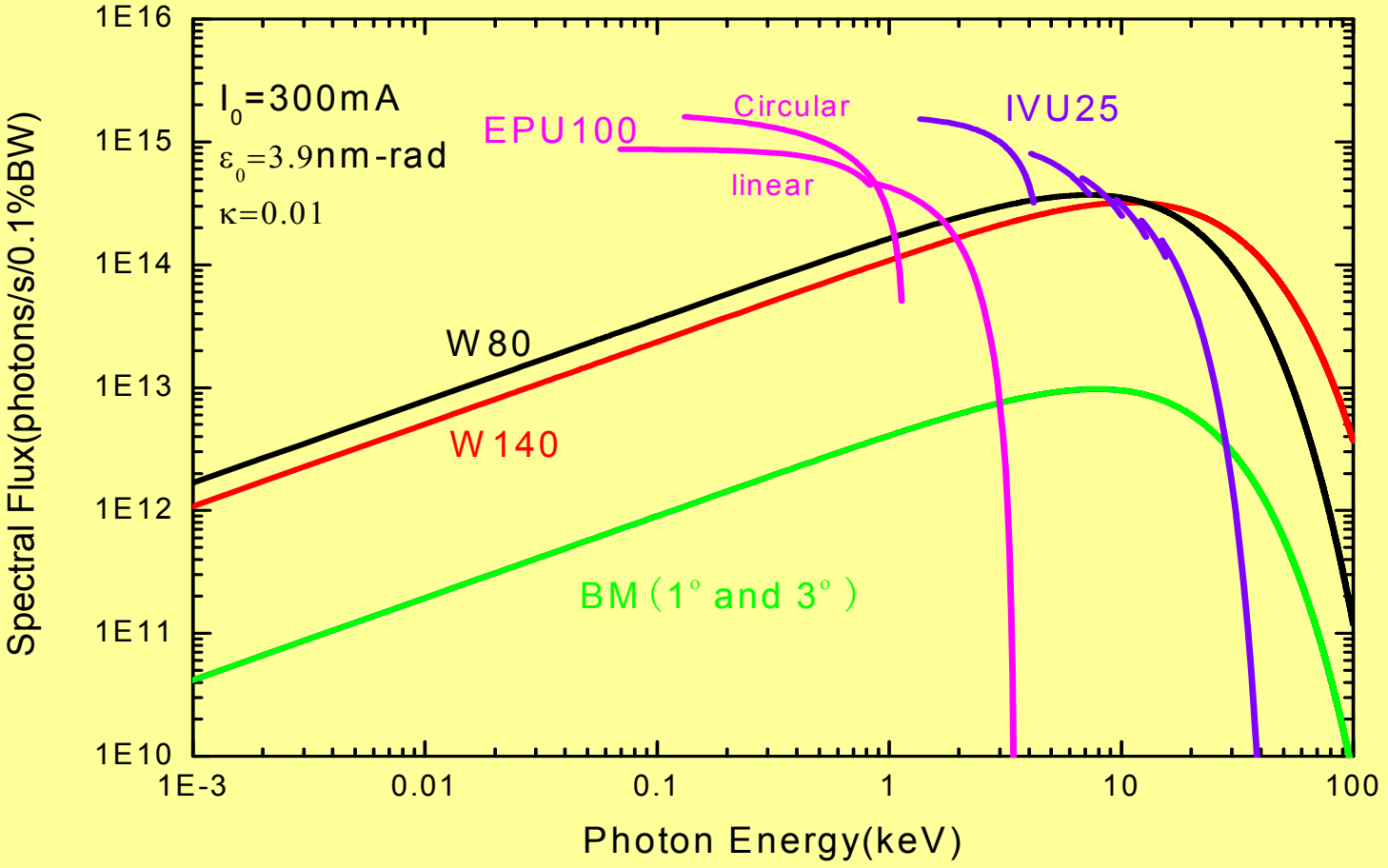

By using superconducting wiggler, the energy range can extend to 300keV

SSRF Phase I Beamlines

- Macromolecular Crystallography Beamline(IVU25)
- Diffraction Beamline (BM)
- XAFS Beamline (Wiggler, W80)
- Hard X-ray Microfocusing Beamline(IVU25)
- X-ray Imaging Beamline (wiggler, W140)
- Small Angle X-ray Scattering Beamline (BM)
- Soft X-ray Spectromicroscopy Beamline (EPU)

All the insertion devices were designed, assembled and tested by SSRF team.

Beamline Specifications

Beamline	Source	Photon energy(keV)	Energy resolution (ΔE/E)	Flux	Spot size(H×V) Spatial resolution
Macromolecular Crystallography	IVU	5~18	≤2×10^{-4}	4.1×10^{12}	67×23 μm^2
XAFS	Wiggler	4~23	<2×10^{-4}	3.6×10^{12}	0.16×0.1mm^2
X-ray Diffraction	BM	4~22	1.9×10^{-4}	1.2×10^{11}	0.21 ×0.13mm^2
X-ray Imaging	Wiggler	9~65	1.6×10^{-3}	1.6×10^{10}	50×50mm^2(spatial resolution<1.0μm)
Hard X-ray Micro-focus	IVU	5~20	1.4×10^{-4}	1.1×10^{11}	0.12× 0.13 μm^2
SAXS	BM	4~22	5.3×10^{-4}	3.0×10^{11}	0.39×0.48mm^2
Soft X-ray Spectromicroscopy	EPU	0.2~2.2	17900@244eV	2.2×10^{8}	30nm

SSRF Construction Schedule and Milestones

- Dce.25, 2004 Ground Breaking
- Dec. 2004 ~ May 2007: Building construction
- Jun. 2005 ~ Jun. 2008: Accelerator equipment and components manufacture and assembly
- Dec. 2005 ~Dec. 2008: Beamline construction and assembly
- May. 2007 ~ Jul. 2007: Linac commissioning
- Oct. 2007 ~ Dec. 2007: Booster commissioning
- Dec. 2007 ~ Dec. 2008: Storage ring commissioning
- Dec. 24, 2007, First SR Light Achieved
- May 2008 ~ Apr. 2009: Commissioning of beamlines
- April 29, 2009: Completion Ceremony
- May 2009: Open to users

SSRF Completion Ceremony, April 29, 2009










Linac

Booster

Storage Ring and IVU25B

EPU

SSRF Experimental Hall

The Status of SSRF Operation

Machine Operation

1. Decay mode: Before December of 2012

210mA → 140mA , two injections per day

2.Top-up mode: From Dec. 6, 2012

(220-1)mA, 10s injection time/ per 10 minutes

Beam current has been increased to 240mA recently

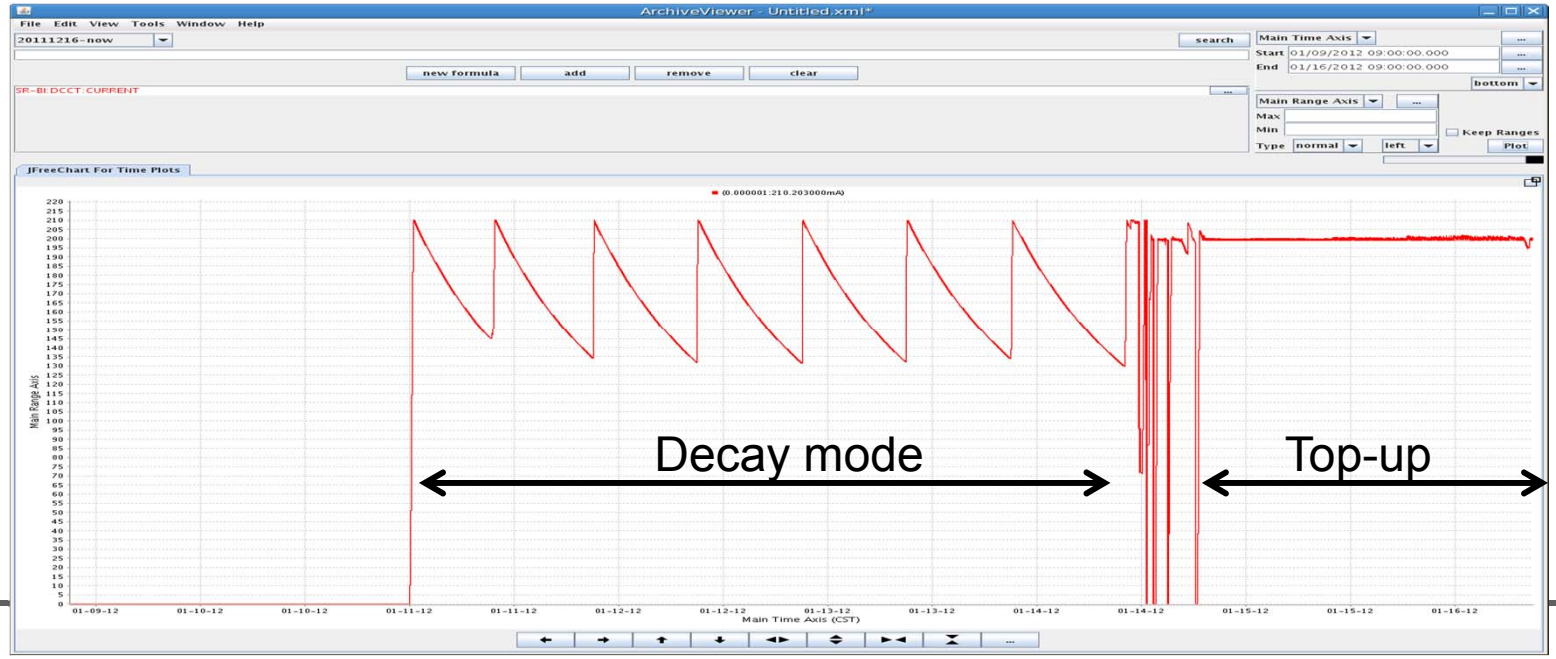

Top-up: Orbit stability

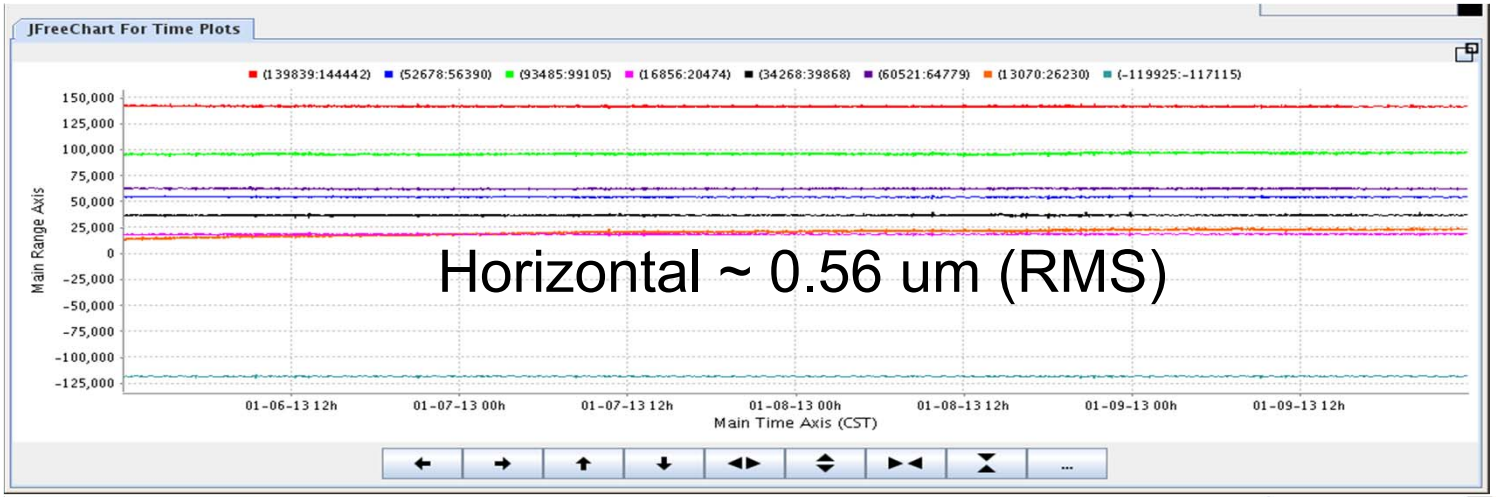

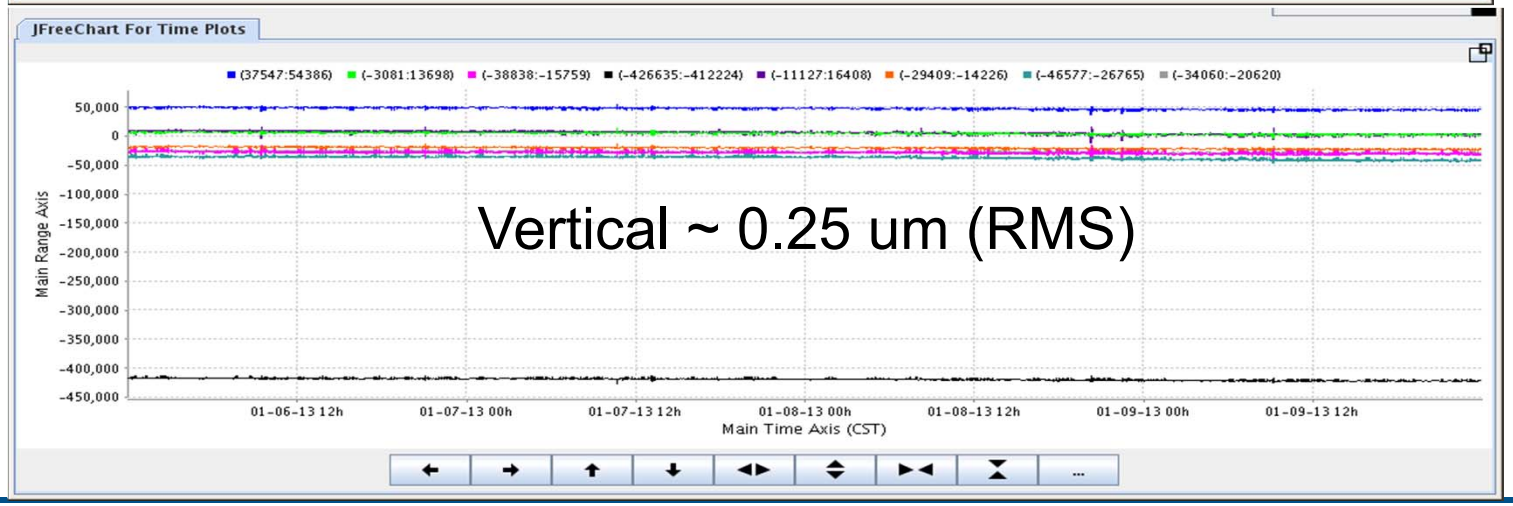

SSRF Accelerator and Beamline Operation

	Accelerator Operation Time (hrs)	Availability (%)	MTBF (hrs)	Beamtime for beamline (hrs)	Beamtime for User (hrs)
2010	7499	96.1	43.7	5507	4000~4500
2011	7644	97.6	55.3	5441	4000~4500
2012	6816	98.4	69.8	5409	4000~4500

Long shutdown(3 weeks longer than usual) in 2012 for the installation of new beamlines

User Activities

Submitted / Approved Proposals for Beamtime

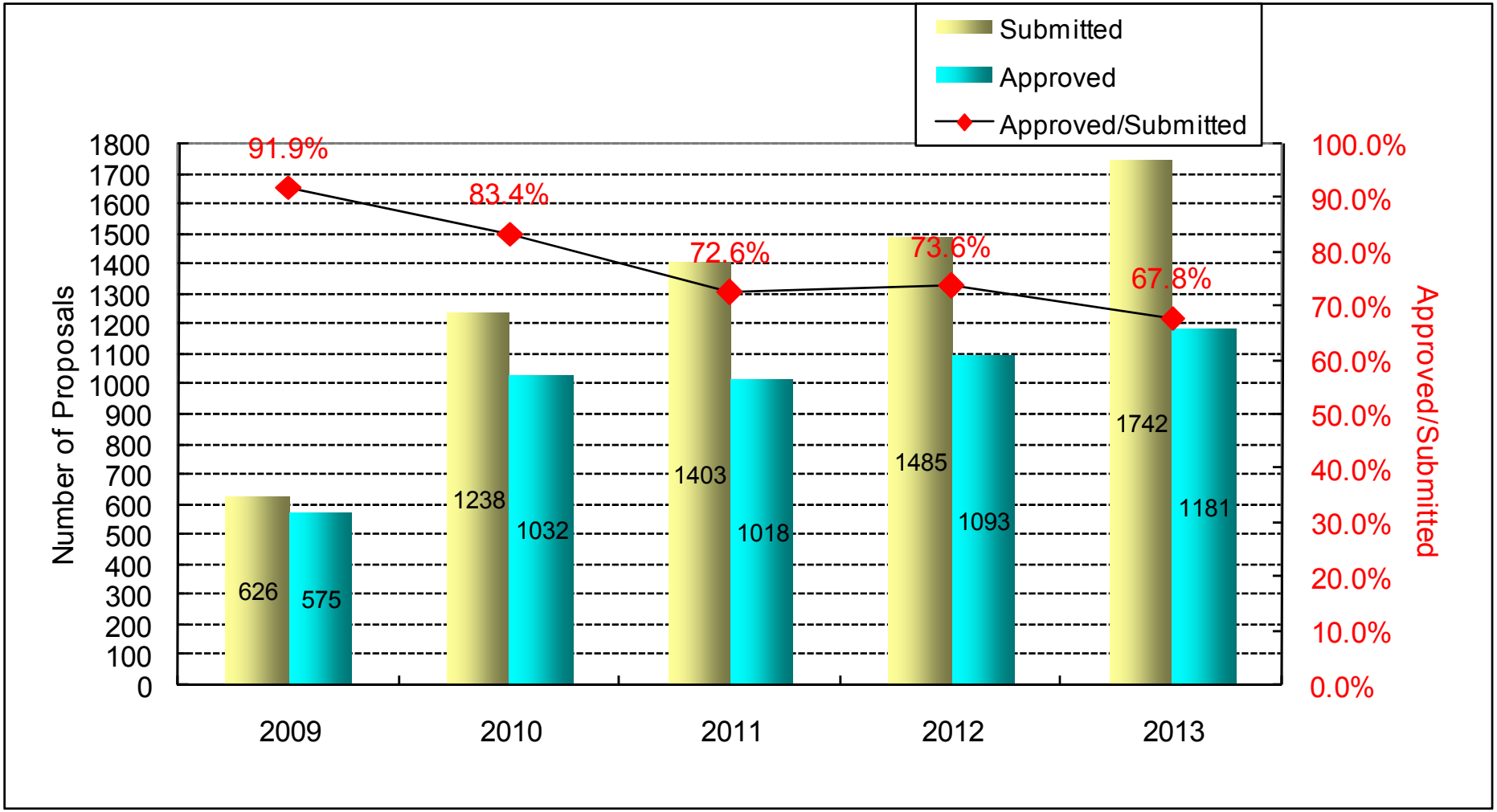

We collect user proposals twice in an year

User Activities

Requested / Allocated Shifts of Beamtime

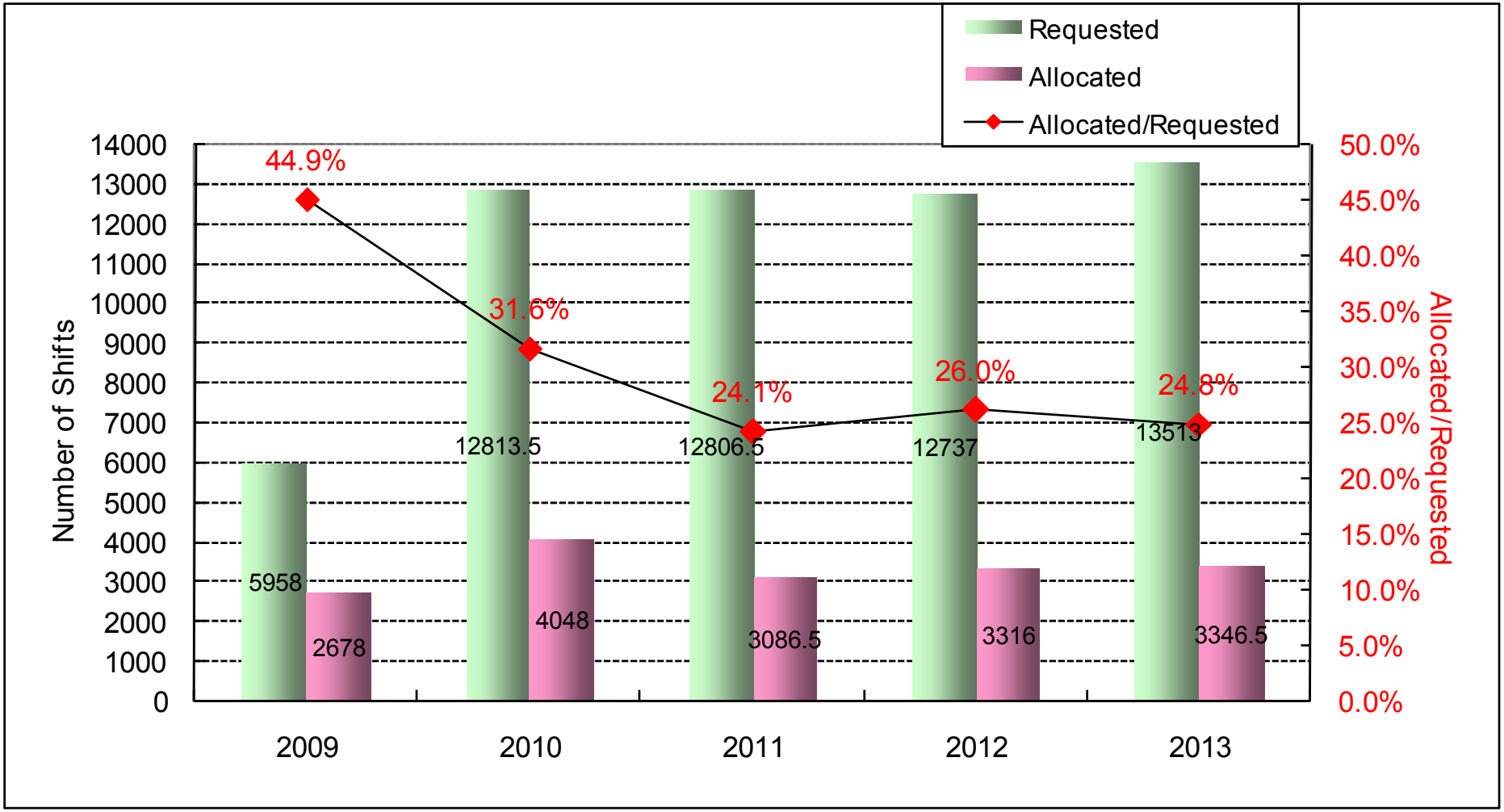

We try to accept more proposals with reduced beamtime

Submitted/Approved Proposals for Beamlines in 2013

Requested/Allocated Shifts for Beamlines in 2103

Research groups and the number of users

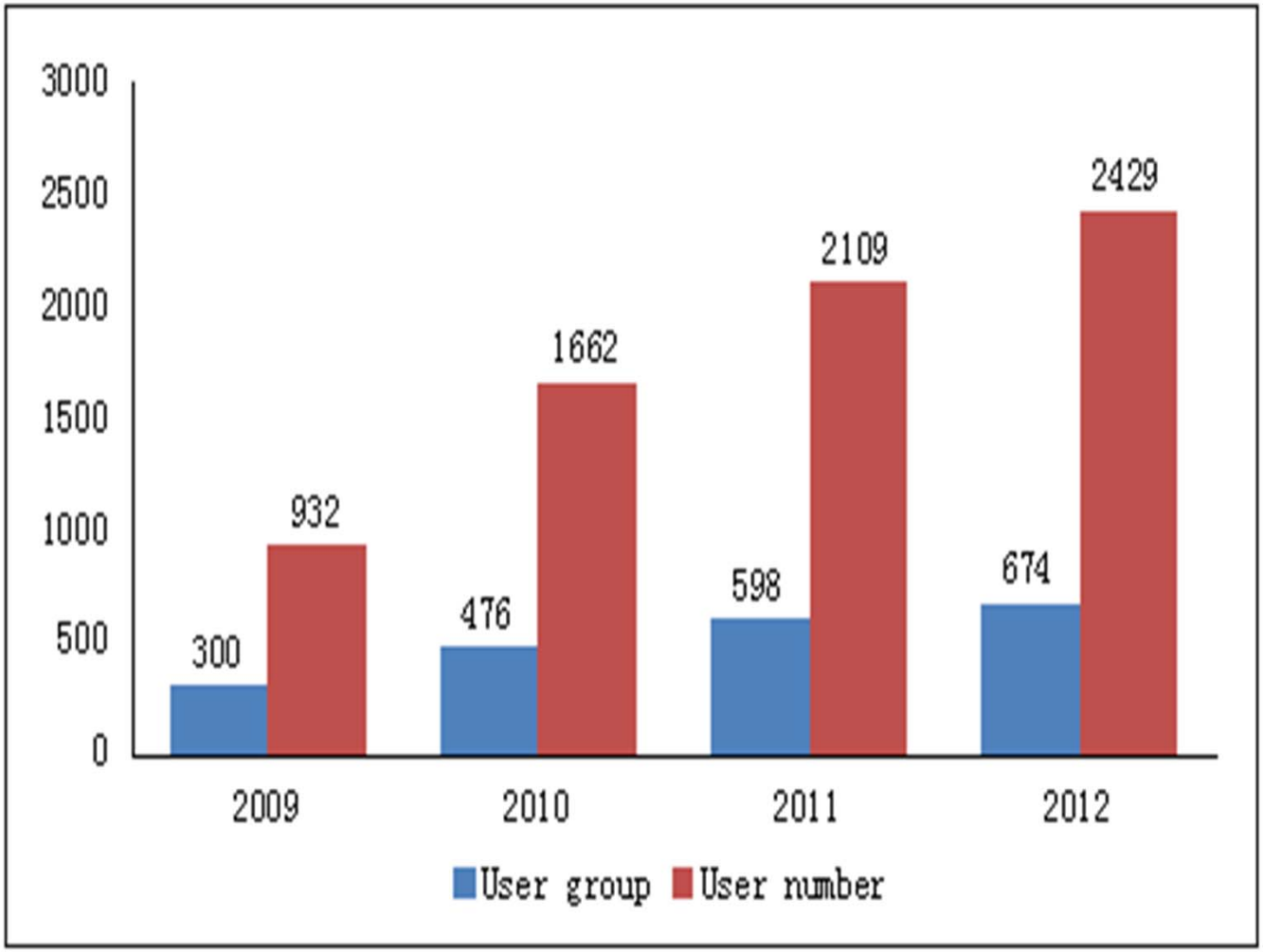

Distribution of users' research fields

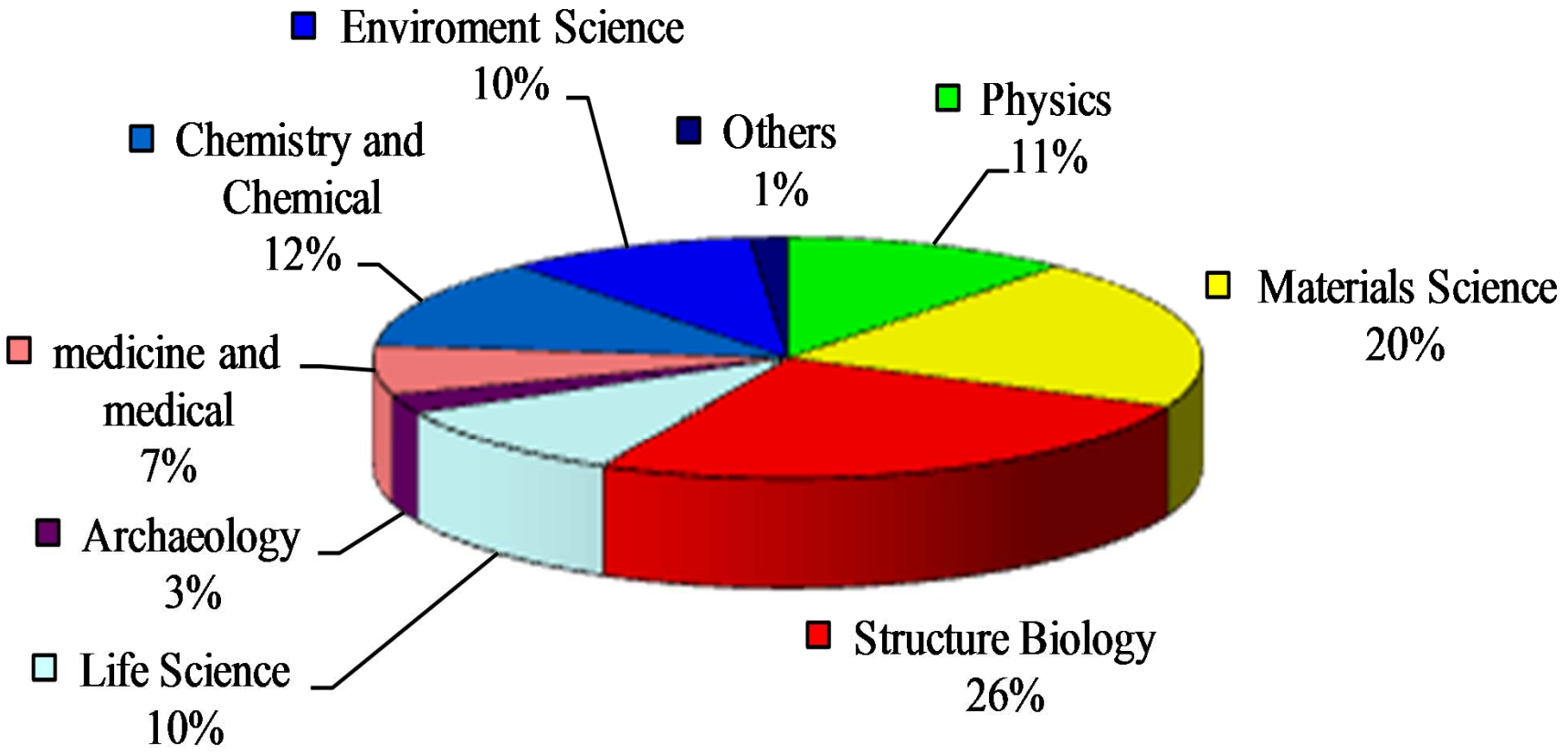

User distribution in regions and institutions (to Nov 30,2013)

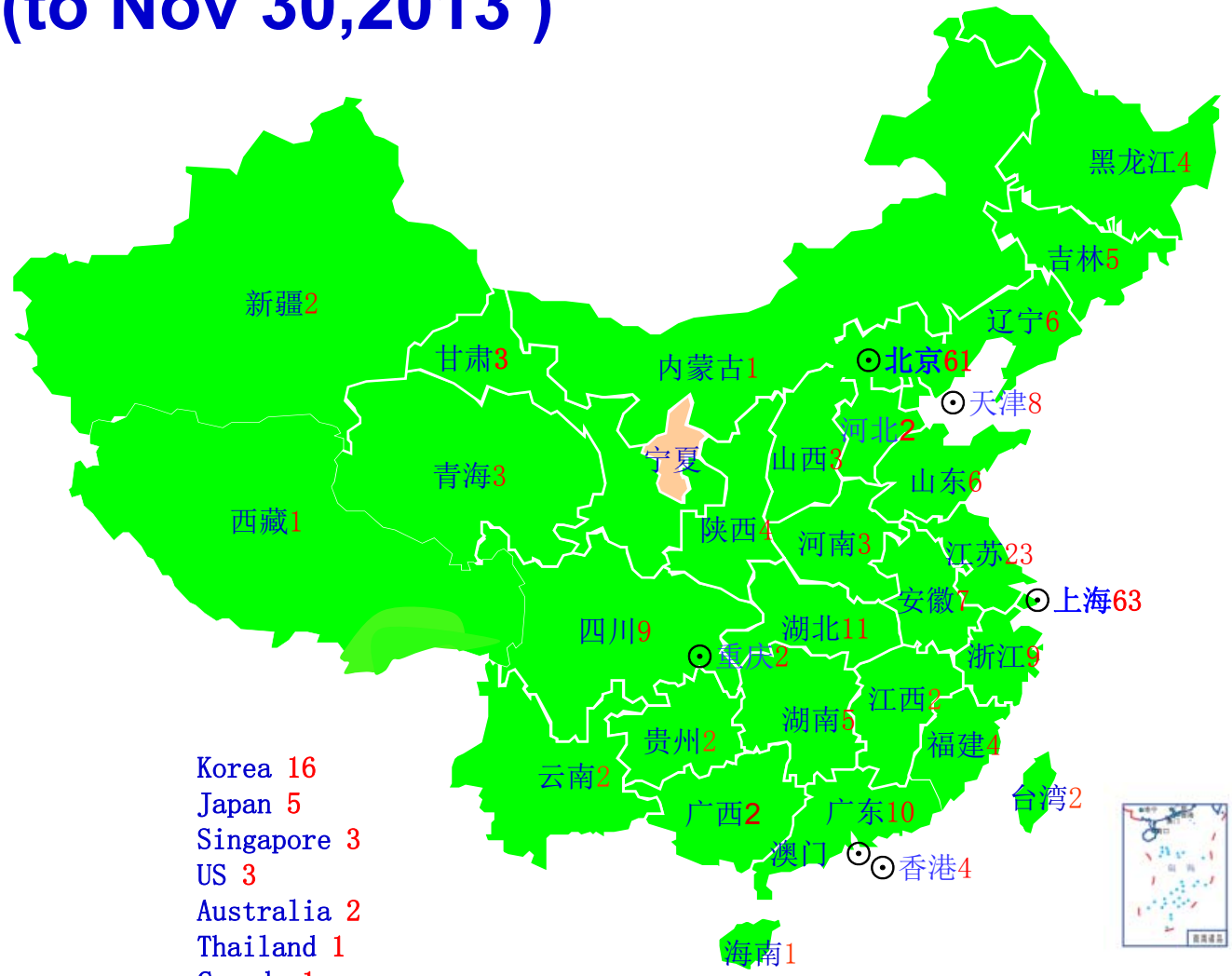

Korea 16
Japan 5
Singapore 3
US 3
Australia 2
Thailand 1
Canada 1
Sweden 1
Denmark 1
Portugal 1

University	147
Institute	105
Hospital	18
Company	33
Total :	303

User Visits: 17612

Users: 7039

Research Publication

Up to Nov of 2013, users have published ~1200 journal papers.

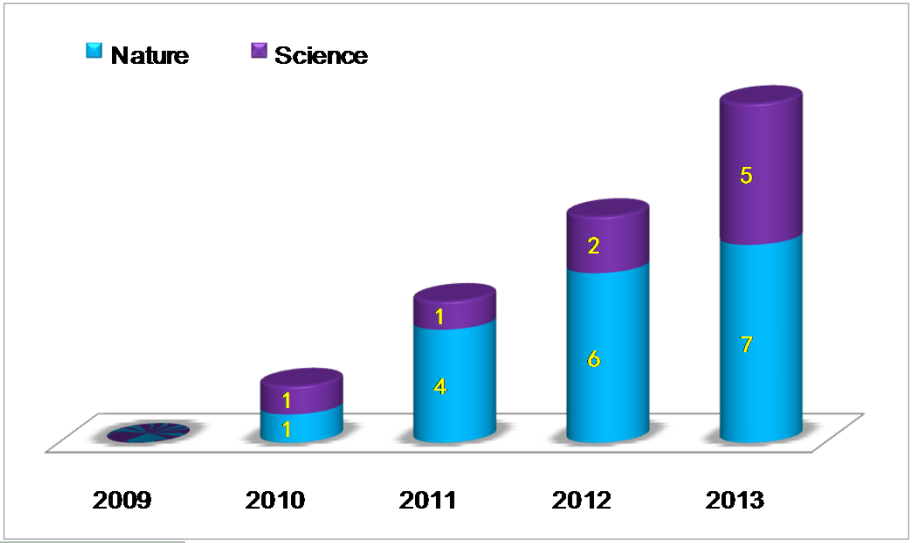

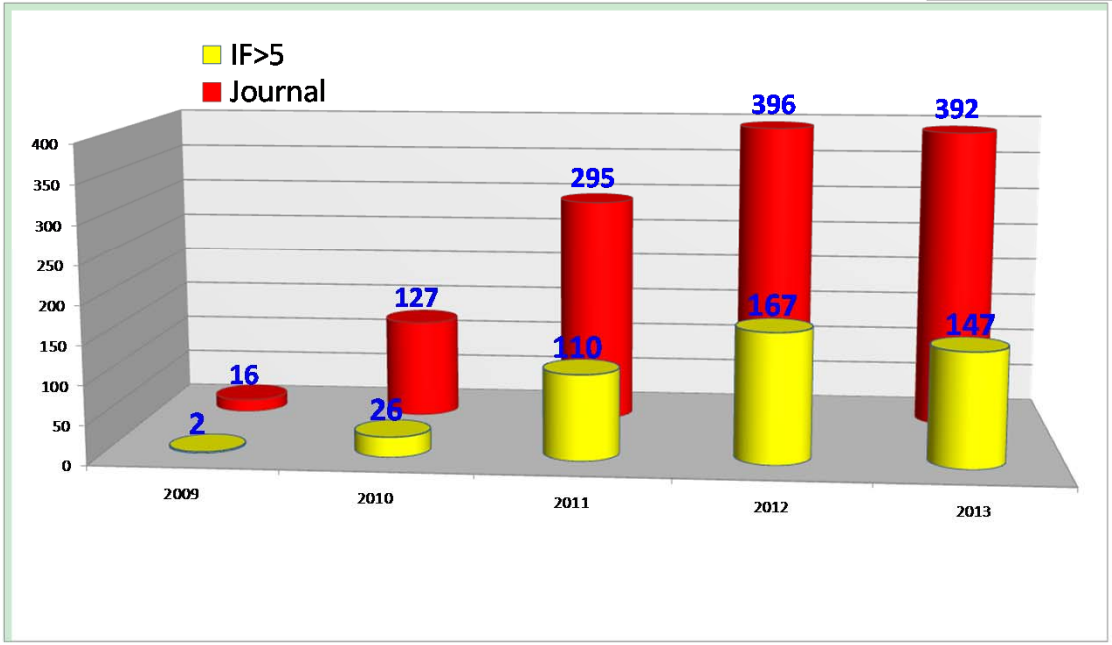

Publications for each year and in top journals keep increasing rapidly

Highlights of User Experiments

Active Research Fields at SSRF

- Structural Biology
- Condensed Matter Physics and Materials Science
- Catalyst
- Environmental Science
- Biomedical and Archaeology Applications

Sequence-Specific Recognition of DNA by TAL Effectors

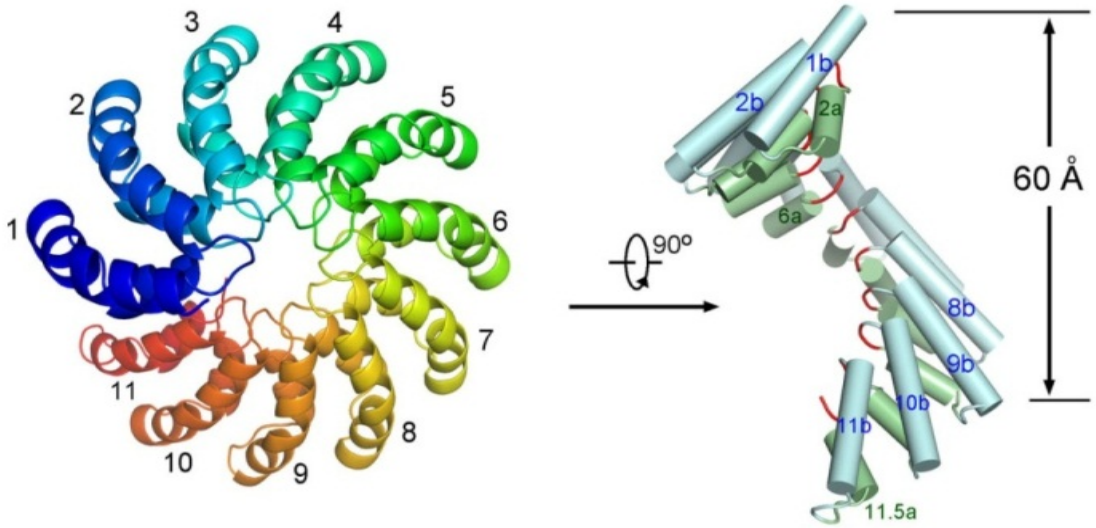

Transcription activator-like effector

Nieng Yan and Yigong Shi's group of Tsinghua University determined the structure of TAL Effectors, which explained the Structural Basis for Sequence-Specific Recognition of DNA by TAL Effectors. *Science (2012)*

- Be referred in "Genomic Cruise Missiles " of "Breakthroughs of 2012" of Science magazine;
- Be selected as "Top 10 Advances in Science" in China in 2012;

Transmission of avian influenza: HxNy

H5N1

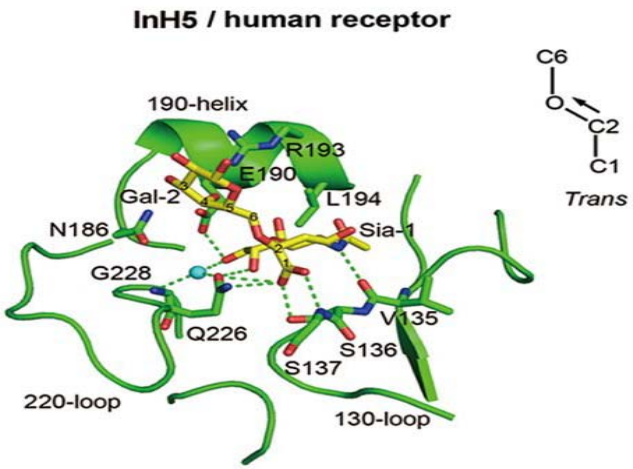

H7N9

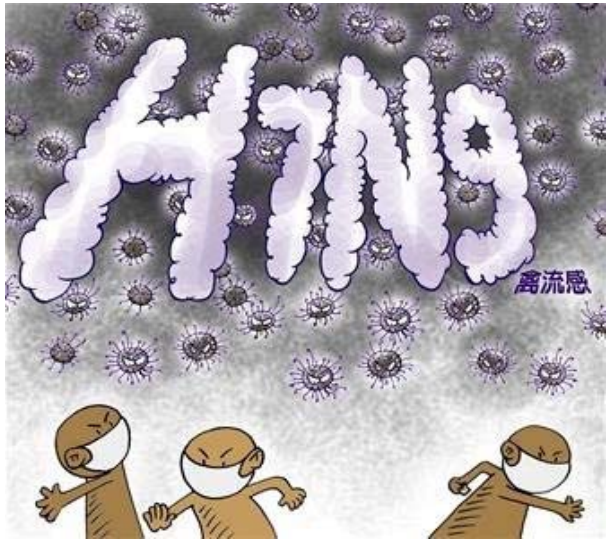

George F. Gao's group of Institute Of Microbiology, CAS/CDC, China

An Airborne Transmissible Avian Influenza H5 Hemagglutinin Seen at the Atomic Level, *Science* : May 3, 2013

Structures and Receptor Binding of Hemagglutinins from Human-Infecting H7N9 Influenza Viruses Science: Sept. 5, 2013

Molecular basis of binding between novel human coronavirus MERS-CoV and its receptor CD26

George F. Gao, Institute Of Microbiology, Nature (2013)

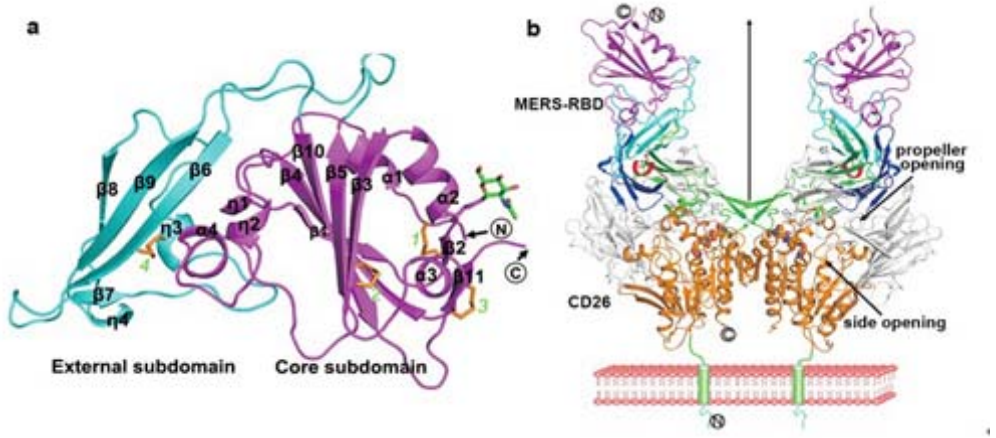

The structure of MERS-RBD and RBD/CD26 complex

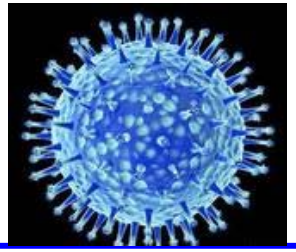

Middle East Respiratory Syndrome coronavirus (MERS-CoV) represents a second reported coronavirus of severely high virulence after SARS-CoV. The clinical manifestations of MERS-CoV infection include fever, cough, acute respiratory distress syndrome and, in some cases, accompanying renal failure, and are very similar to those caused by SARS-CoV.

Researchers identified MERS-RBD protein responsible for binding CD26 firstly. Finally they resolved MERS-RBD and RBD/CD26 complex using BL17U1, respectively. It is important for the drug design.

The energy-coupling factor transporter

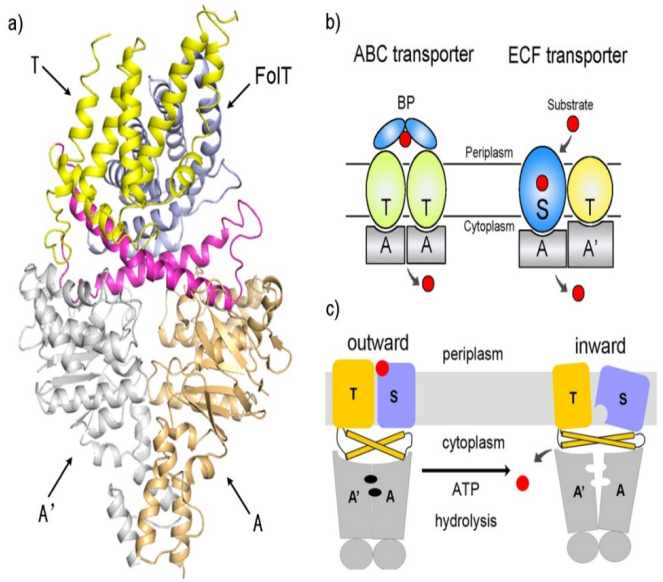

***Nature* 497, 268–271**
Peng Zhang
SIBS, CAS

***Nature* 497, 272–276**
Yigong Shi
Tsinghua University

The energy-coupling factor (ECF) transporters constitute a novel family of conserved membrane transporters in prokaryotes that have a similar domain organization to the ATP-binding cassette transporters. Using BL17U1, they determined the structure of ECF transporters propose a transport model that involves a substantial conformational change of ECT transporters.
Because this transporter only exist in bacteria, the protein can be targets for the design of new antimicrobial drugs.

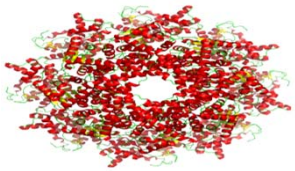

Crystal structure of
Caenorhabditis elegans apoptosome
Cell 141, 446-457

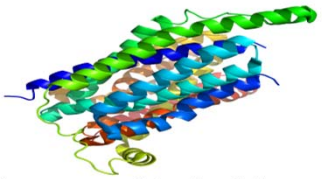

Crystal structure of the E.coli Fucose:proton symporter, FucP (N162A)
Nature 467, 734–738

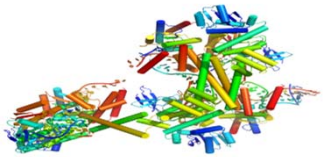

Crystal structure of a catalytically active substrate-bound box C/D RNP from *Sulfolobus solfataricus*
Nature 469, 559-563

Structure of myosin VIIa MyTH4-FERM-SH3 in complex with the CEN1 of Sans
Science 331, 757-760

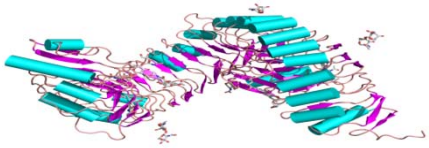

Crystal structures of BRI1 and brassinolide complex
Nature 474, 472-476

Structure and mechanism of the hexameric MecA–ClpC molecular machine
Nature 471, 331-335

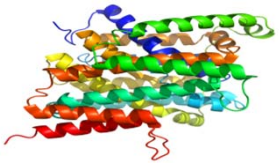

Structure of the uracil transporter UraA
Nature 472, 243-246

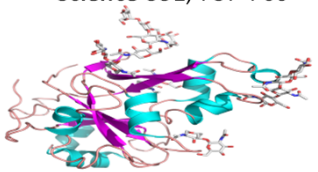

Crystal structure of the ectodomain of a receptor like kinase
Science 336, 1160-1164

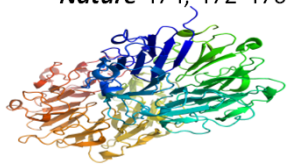

Crystal structure of the W285F mutant of UVB-resistance protein UVR8
Nature 484, 214-219

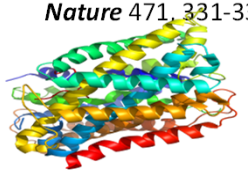

Structure of glutamate-GABA antiporter GadC
Nature 483, 632-636

Structure of an orthologue of the NaChBac voltage-gated sodium channel
Nature 486,130–134

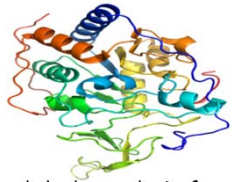

The novel de-long chain fatty acid function of human sirt6
Nature 484, 214-219

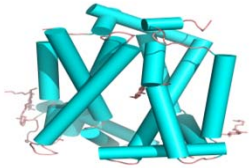

The structure of the MFS proton:xylose symporter XylE bound to D-glucose
Nature 490, 361-365

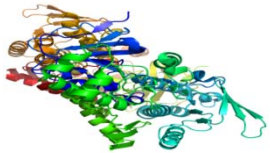

Crystal structure of NDH with NADH
Nature 491, 478-482

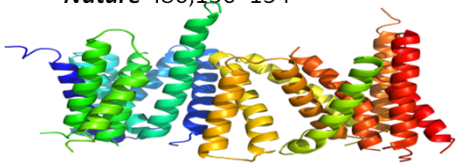

Structure of a presenilin family intramembrane aspartate protease
Nature 493, 56-61

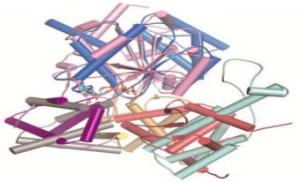

Crystal Structure of NLRC4 Reveals Its Autoinhibition Mechanism
Science 341, 172-175

SSRF MX beamline:
27 papers have been published in Nature, Science and Cell

So far, 818 structures published in PDB.
320 structures solved in 2012, ranking 1st in over 130 MX beamlines worldwide

Re-emerging superconductivity at high pressure in iron chalcogenid（High Prssure μ-XRD）

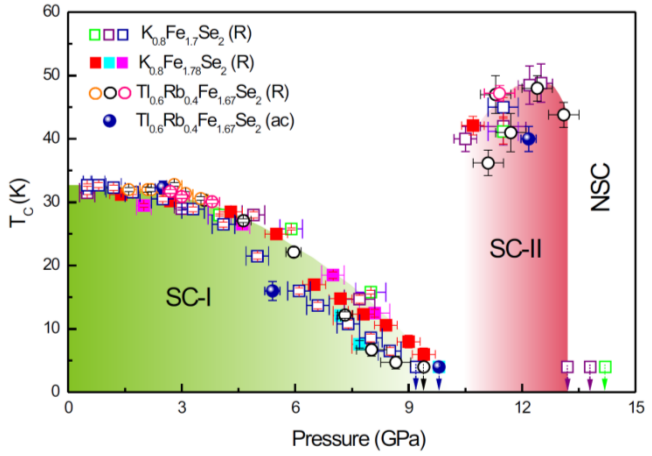

New Tc record 48K @12.5GPa

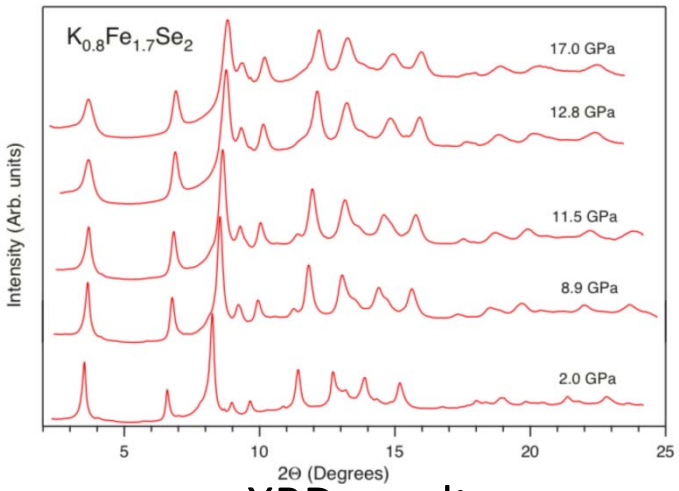

μ-XRD results

Pressure induced superconducting phase has be discovered and this phenomena is related to quantum criticality.

Lilin Sun et al., IOP CAS
Nature 483, 67–69 (2012)
Physical Review Letters, 108, 197001 (2012)

RSM study of Ferroelectric tunnel junctions

Ferroelectric tunnel junctions (FTJs), composed of two metal electrodes separated by an ultrathin ferroelectric barrier, have attracted much attention as promising candidates for onvolatile resistive memories. Professor Wu Di from Nanjing University propose a novel tunnelling heterostructure by replacing one of the metal electrodes in a normal FTJ with a heavily doped semiconductor.

Reciprocal space mapping(RSM) around the (013) Bragg reflection of Pt/BaTiO3/Nb:SrTiO3 indicates coherent growth of BTO on Nb:STO substrates.

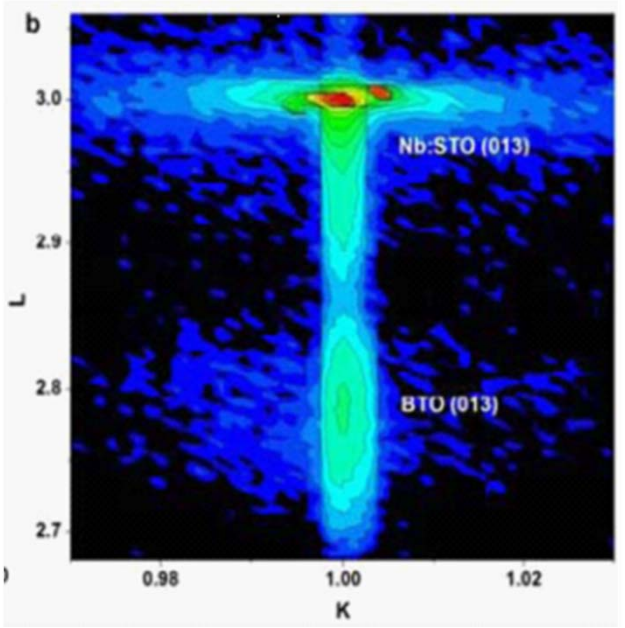

RSM of $Pt/BaTiO_3/Nb:SrTiO_3$

Three-Dimensional Coherent X-Ray Diffraction Imaging of Molten Iron in Mantle Olivine at Nanoscale Resolution

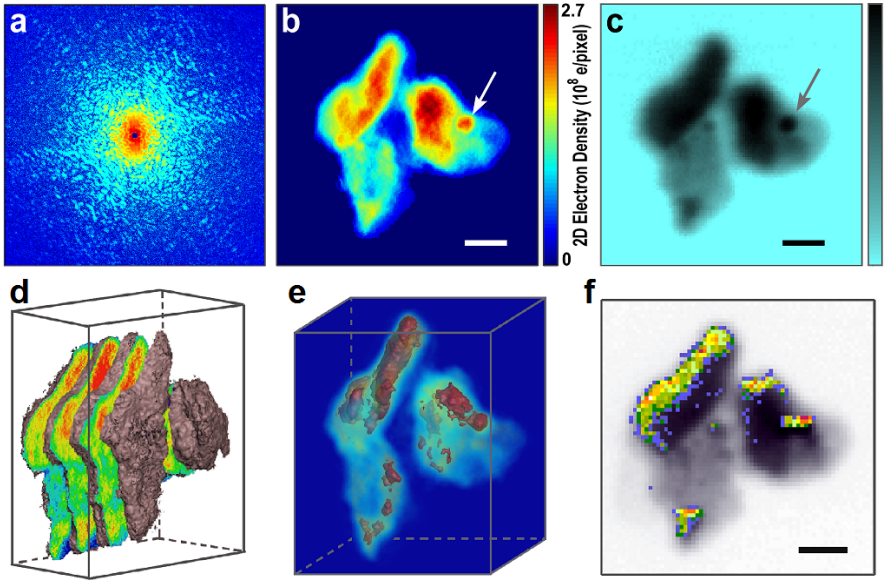

(a) A representative coherent x-ray diffraction pattern measured from an olivine-Fe-S sample. (b) A 2D projection of the olivine-Fe-S sample reconstructed from (a), showing different electron density. (c) STXM image of the same sample and (f) (b) 2D dual-energy STXM image near the Fe L3 edge: 703.75 eV and 709 eV. The colored areas indicate the existence of the Fe-rich phase within the sample. Scale bar is 500 nm.

CDI and STXM measurements of molten Fe-rich alloy and mantle olivine were used to investigate the 3D melt distribution at the nanoscale resolution. CDI provides 3D local structure at high resolution, while STXM offers the element-specific imaging capability. The combined results provide direct evidence of the existence of 3D Fe-rich and Fe-S phases in the olivine-Fe-S sample at the nanoscale resolution.

Physical Review Letters, 2013, 110: 205501

Huaidong Jiang group, Shandong University

Liquid Crystals of Graphene Oxide

As a new two-dimensional material, graphene, a single layer of graphite, has attracted considerable attention. Now, how to fabricate graphene-based materials with ordered structures is becoming an important but challenging task. Gao's group from Zhejiang University **tracked the evolution of phase state in the graphene oxide liquid crystals by Synthrotron SAXS**. **The results explain the structural evolution from isotropic to nematic and lamellar mesophase of graphene oxide liquid crystals depending on the concentrations.**(Aqueous Liquid Crystals of Graphene Oxide.

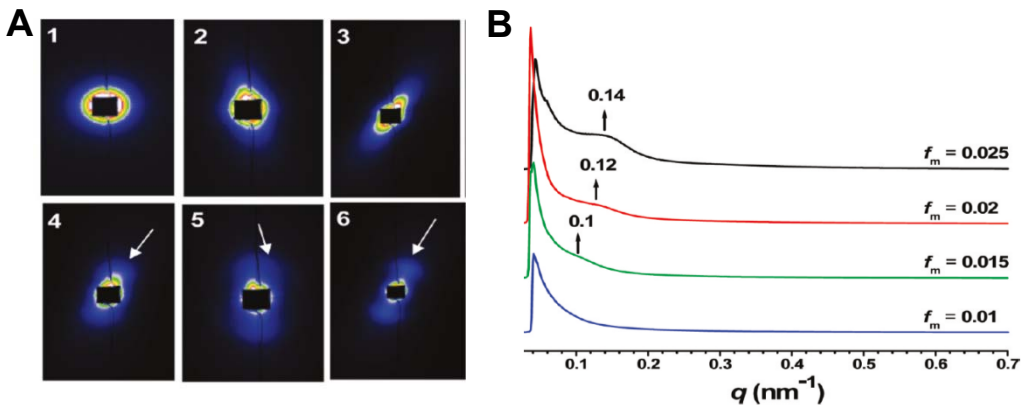

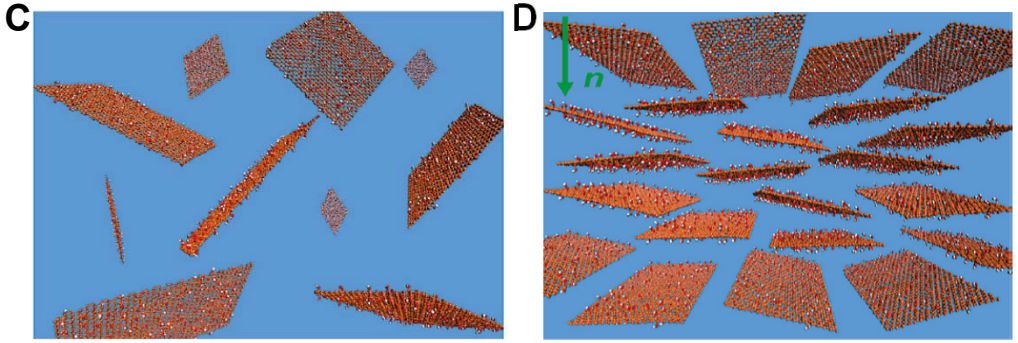

ACS Nano, 2011,5 (4), 2908-2915)
C. Gao et al., Zhejiang University

(A) SAXS 2D patterns of *GO* aqueous dispersions with *increasing concentration from 1-6.*

(B) *SAXS* profiles of liquid crystals of *GO* with high concentrations.

(C) and (D) are schematic models for isotropic and nematic phases of graphene oxide aqueous dispersions,respectively.

Ultrastrong Graphene Fibers

(Gao Chao of Zhejiang Univ.)

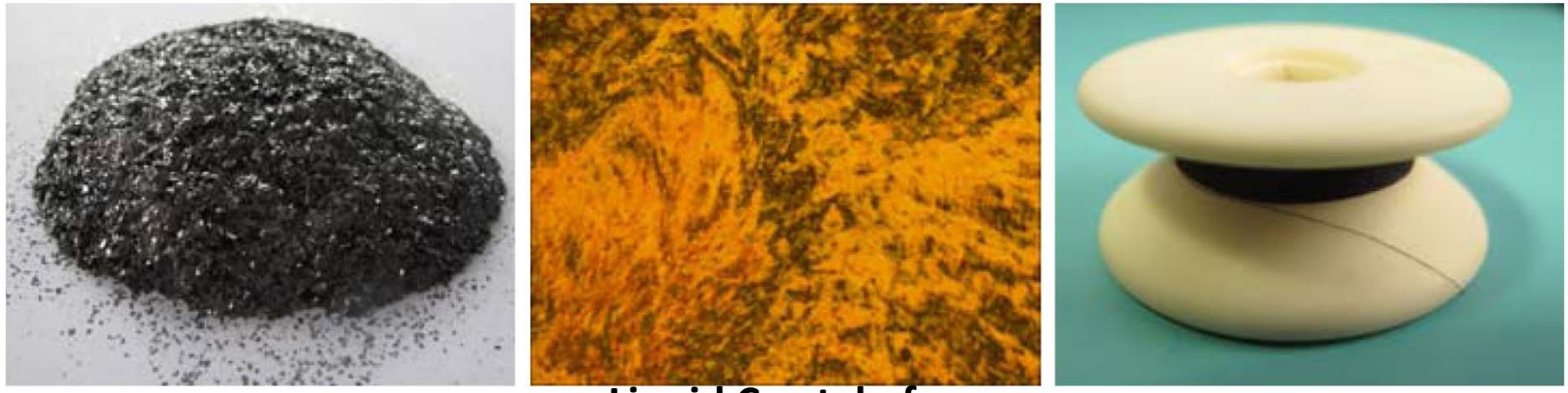

Graphite → **Liquid Crystal of Graphene oxide** → **Graphene Fiber**

The Gao's group prepared giant graphene oxide (GGO) sheet and comfirmed its liquid crystal phase in aqueous by **the SAXS characterization of SSRF**. Continuous, ultrastrong graphene fibers were subsequently spun from GGO.

The graphene fibers possessed **a record tensile strength (up to 0.5 GPa)** among neat graphene materials, with excellent electrical conductivity. Such multifunctional graphene fibers have promise **in versatile applications** such as functional textiles, flexible and wearable sensors, and supercapacitors devices.

This work was published in Advanced Materials and highlighted by 'Materials Views China' entitled with 'Continuous, Ultrastrong Graphene Fibers from Graphite'.

Materials Views 中國

WILEY Publishers Since 1807

GIXRD study of High-Performance Organic Solar Cells

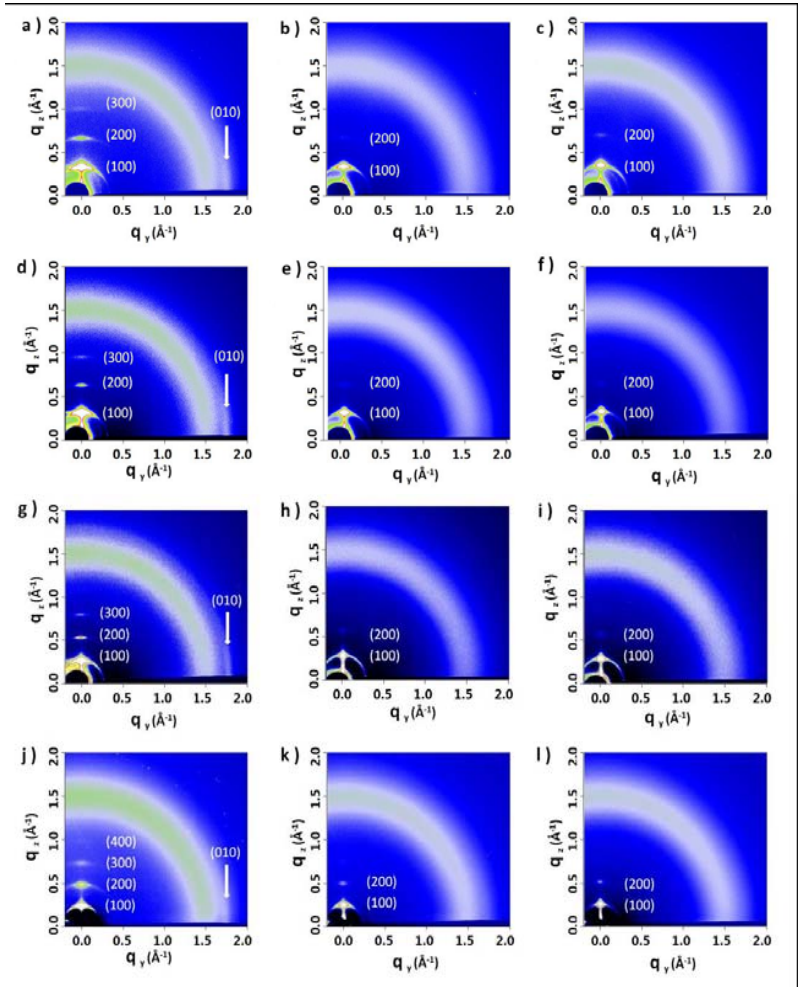

2D GIXRD of DR3TBDTT, DR3TBDTT-HD, and DR3TBD2T

☞The 2D GIXRD results indicated the donor domain sizes of the compounds (DR3TBDTT, DR3TBDTT-HD, and DR3TBD2T) were 10−20 nm. Furthermore all of the compounds exhibited a greater preference for edge-on molecular orientation relative to the substrate.

J. Am. Chem. Soc., 2013, 135 (23), pp 8484–8487

Nano-catalyst

CO Oxidation using Fe-based catalyst

Interface-Confined Ferrous Centers for Catalytic Oxidation

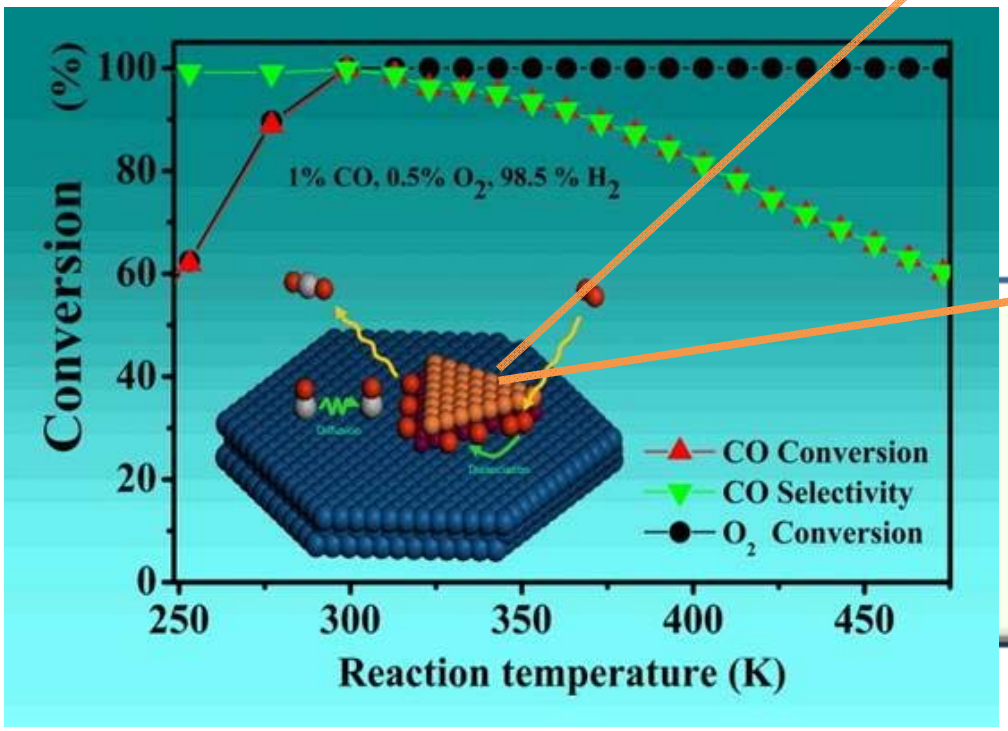

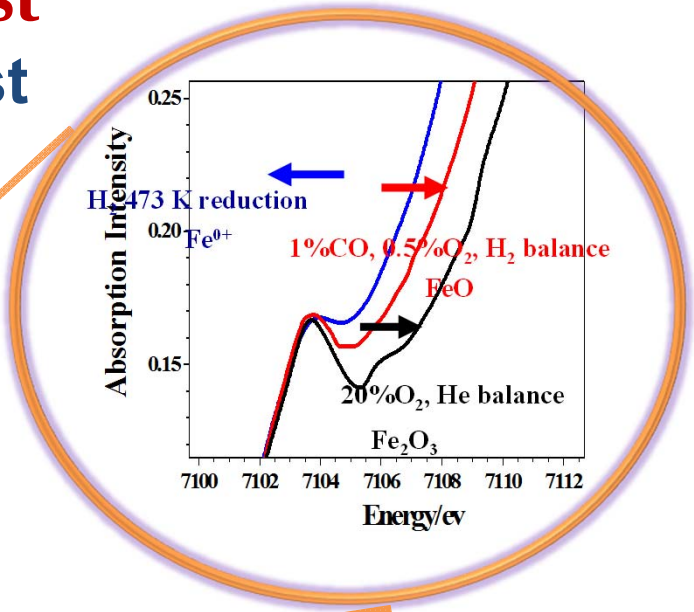

The in-situ oxidation of Fe at the interface of FePt nanoparticles was determined by XAFS technique.

Demonstrated the mechanism of this type of catalyst

Xinhe Bao, Qiang Fu et al., Dalian Institute of Chemical Physics, CAS

Science, 328, 1141 (2010)

Single-atom catalysis of CO oxidation using Pt_1/FeO_x

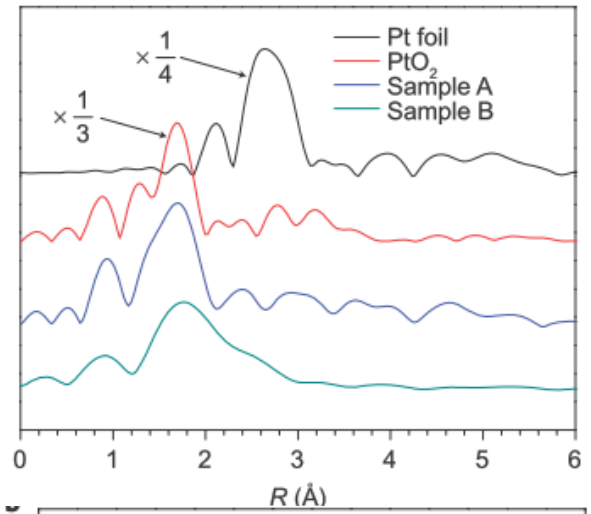

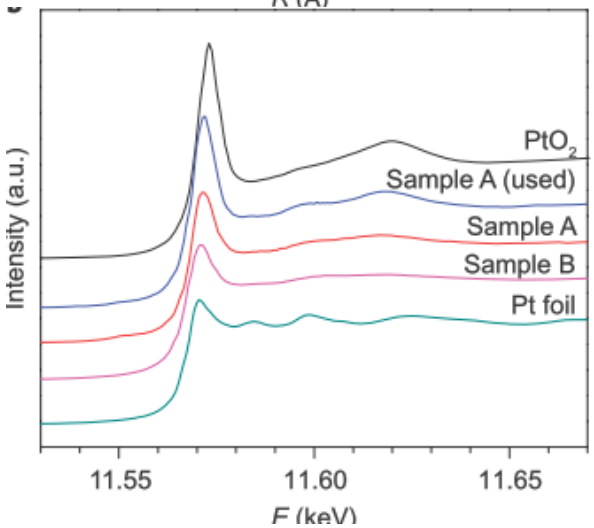

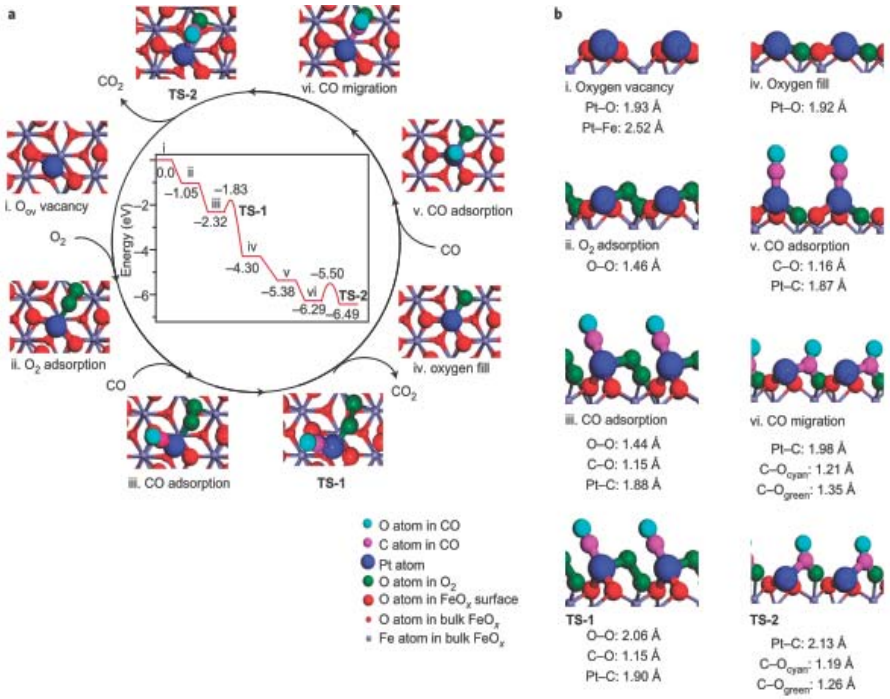

The synthesis of a single-atom catalyst that consists of only isolated single Pt atoms anchored to the surfaces of iron oxide nanocrystallites. This single-atom catalyst has extremely high atom efficiency and shows excellent stability and high activity for both CO oxidation and preferential oxidation of CO in H_2

Tao Zhang, Dalian Institute of Chemical Physics, CAS,

***Nature Chemistry*, (2011) 3,634**

Confinement effect of catalysts within carbon nanotubes

（DICP ,CAS　Xinhe Bao）

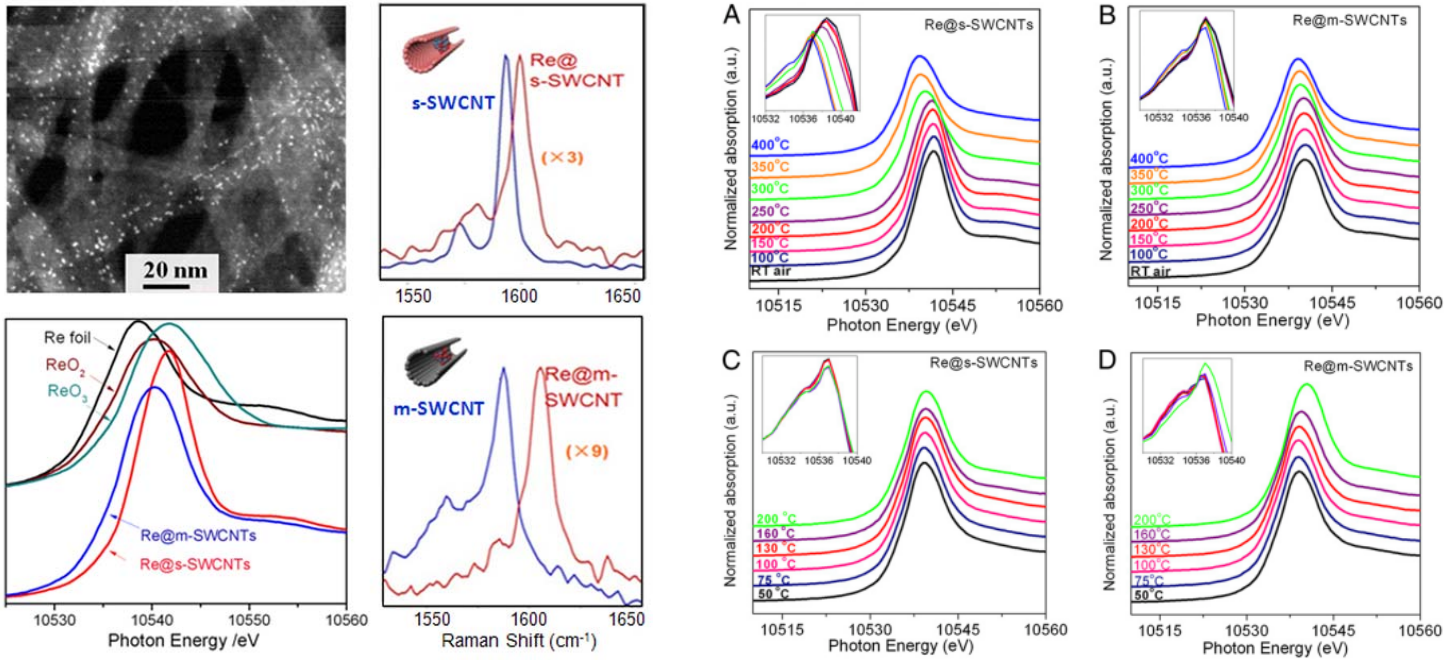

Studies with *in situ* XANES and Raman spectroscopy demonstrate that the reduction and oxidation activities of the encapsulated rhenium species can be modulated by utilization of metallic or semiconducting SWCNT tubes. These results provide a chemical approach to modulate reversibly the electronic structure of SWCNTs without damaging the sidewalls of SWCNTs.

PNAS 110 (37), 14861–14866（2013）

Spatial distribution of arsenic and temporal variation of its concentration in rice **M. Z. Zheng et al.** New Phytologist 189: 200–209 (2011)

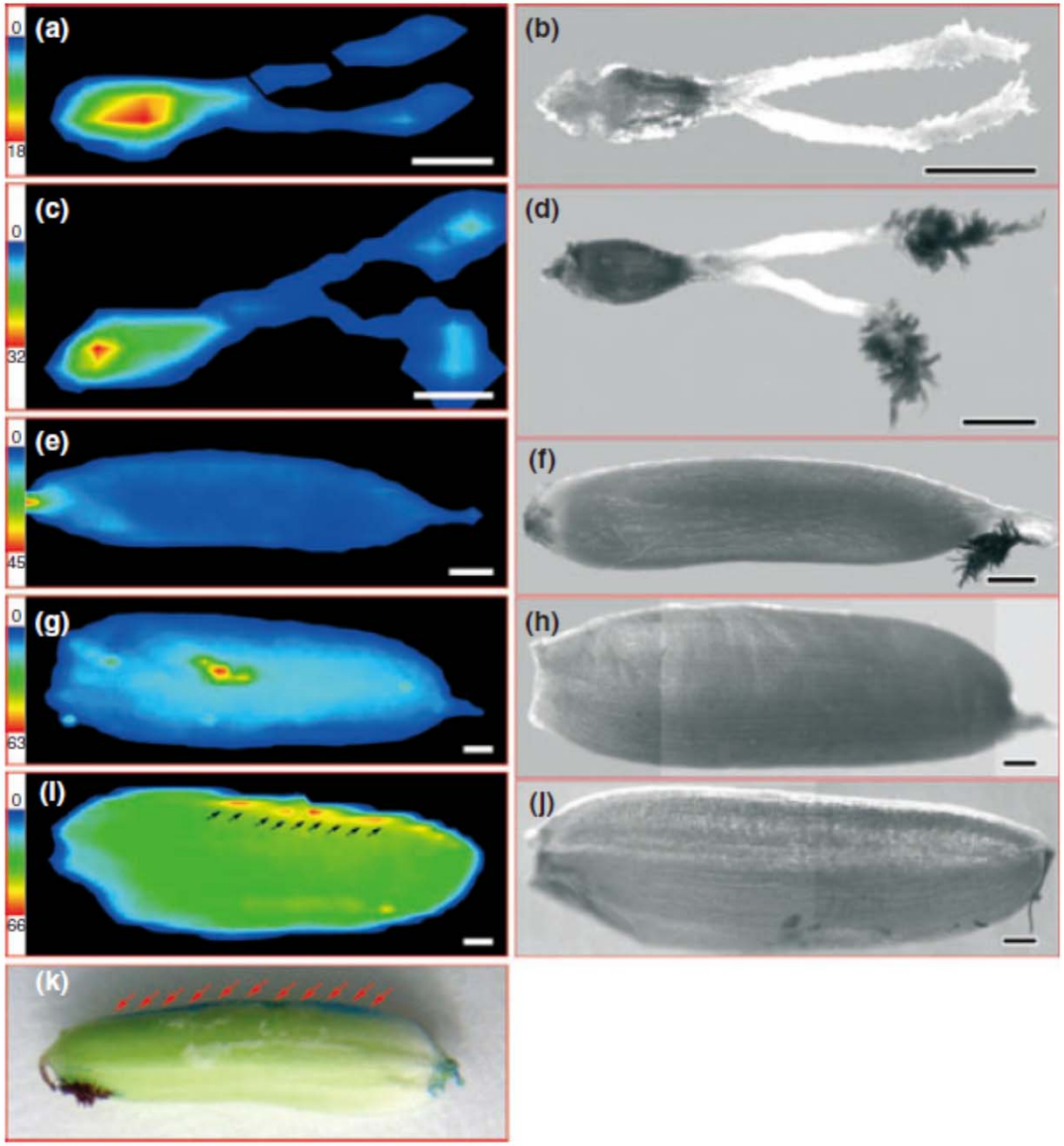

Synchrotron-based X-ray fluorescence (SXRF) was used to map the As distribution in rice (Oryza sativa) caryopses at different developmental stages.

The investigation has, for the first time, documented in detail the spatial distribution and temporal variation of As in the whole rice plant, providing a more global view of the transport of As into grains.

Decreasing south Asian summer monsoon in the past 160 years

Guoqiang Chu et al., Journal of Geophysical Research，D02116（2011-1-26）

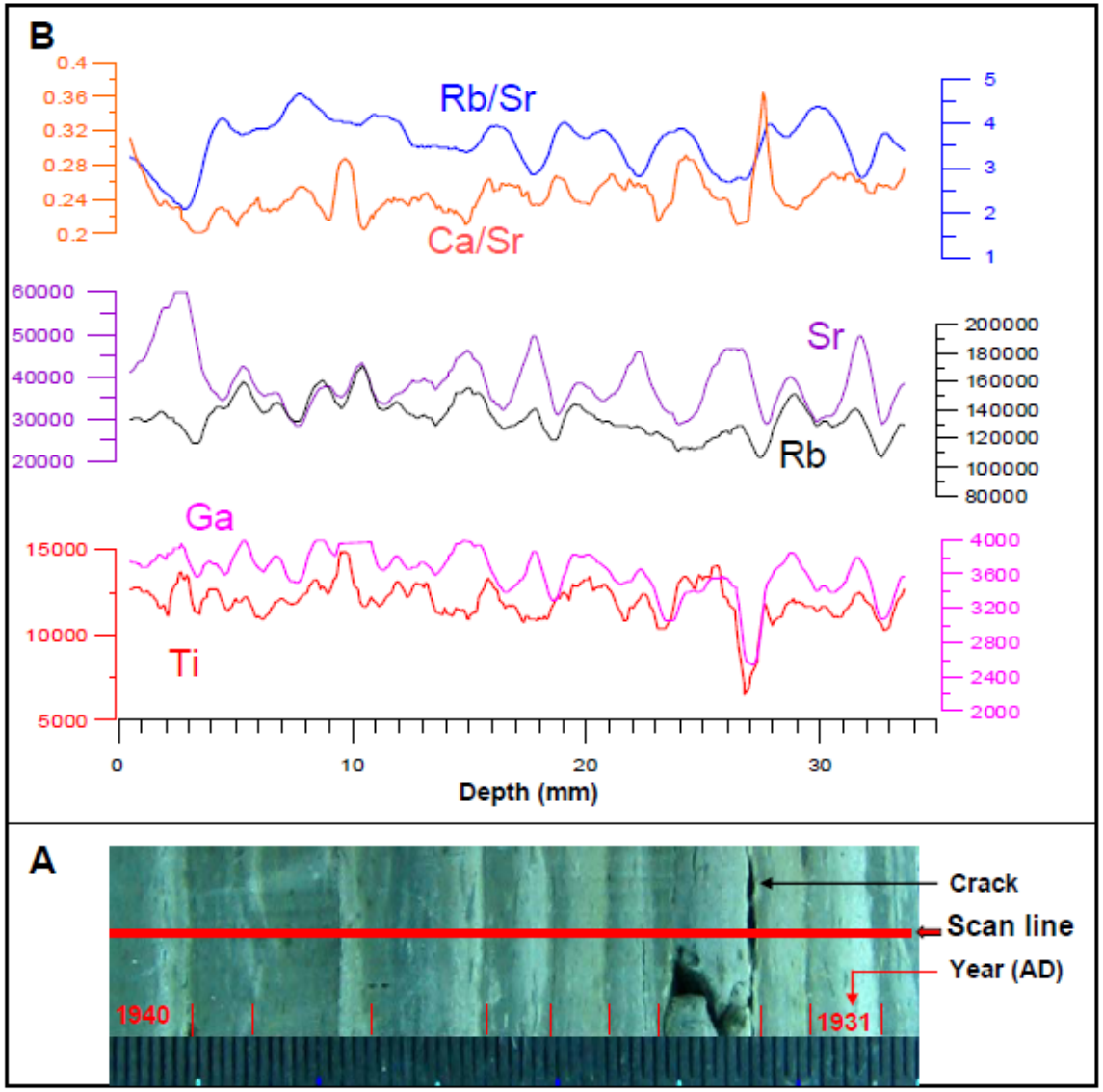

Titanium concentration is good agreement with spring precipitation. Rb/Sr ratio co-varies with the temperature, may be an indicator of chemical weathering.

Decreasing south Asian summer monsoon in the past 160 years from varved sediment in Lake Xinluhai, Tibetan Plateau

Glacial varves in the Tibetan Plateau provide a new window for high-resolution paleoclimatic study in this data-sparse area.

Arsenic Removal and Recovery from Copper Smelting Wastewater Using TiO_2

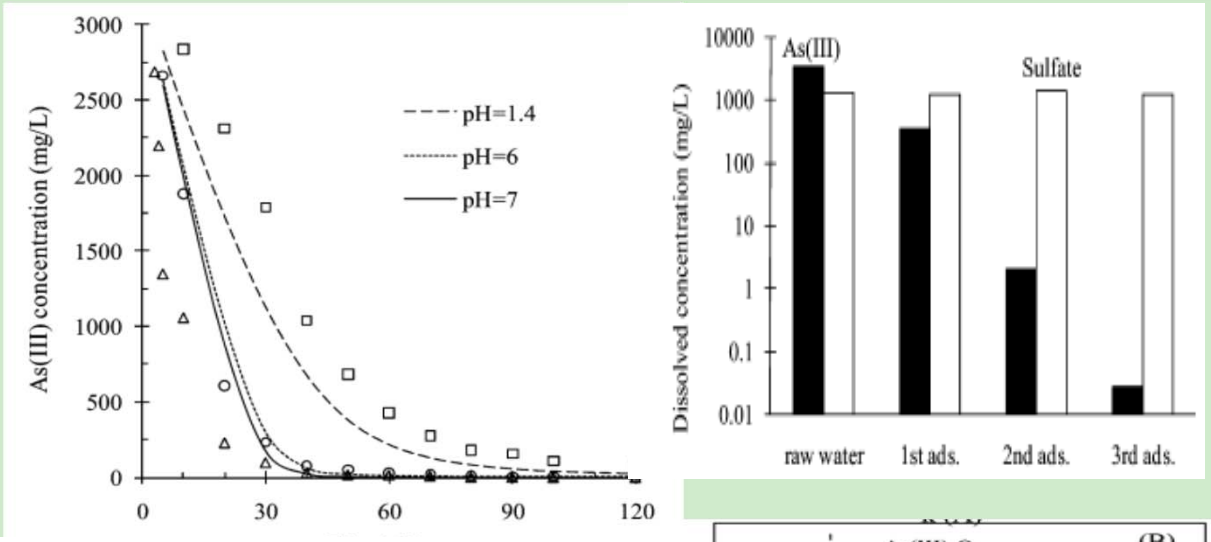

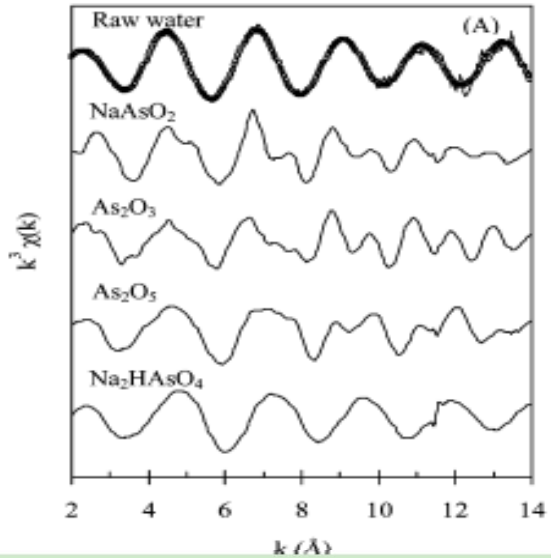

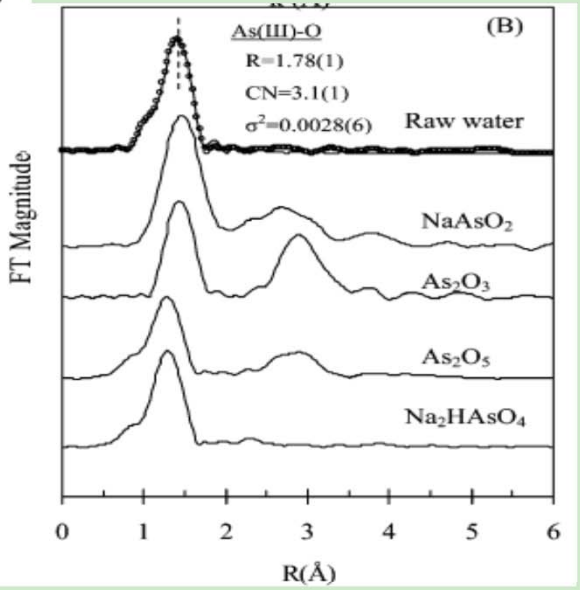

The detailed local structural information of adsorbed As(III) on the TiO2 nanoparticle surface was determined by XAFS technique, revealing the adsorption behavior of As in different pH environment.

Chuanyong Jing et al, Research Center for Eco-Environmental Sciences, CAS,
Environmental Science & Technology， 44, 9094 （2010）

Biomedical Applications

The Application Research of Hard X-ray Phase-Contrast Imaging in Medicine and Pathology

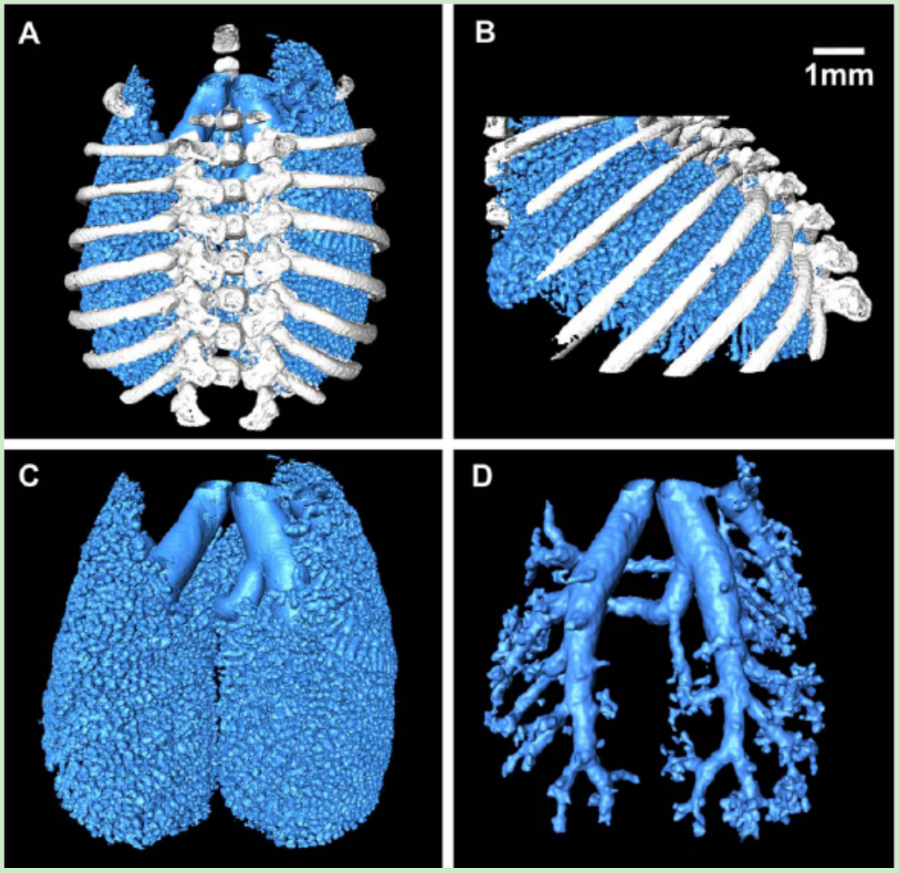

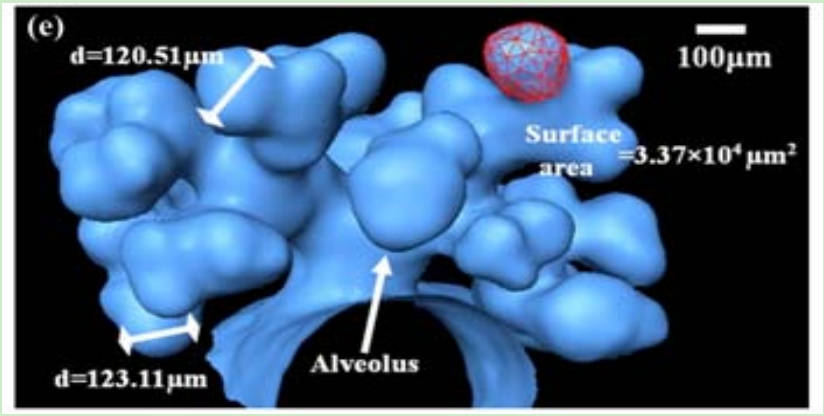

3D lung images of mouse. (A-B) Different views of the lung; (C) The bronchi and alveoli, the 3D model was cut *in order to see the inner part of the lung. (D) The bronchial tree.*

Lu Zhang, Dongyue Li and Shuqian Luo, **"Non-Invasive Microstructure and Morphology Investigation of the Mouse Lung: Qualitative Description and Quantitative Measurement"** Plos One 6, e17400, 2011

Luo Shuqian Group, Capital Medical University

Live imaging of rat middle cerebral artery occlusion(MCAO)

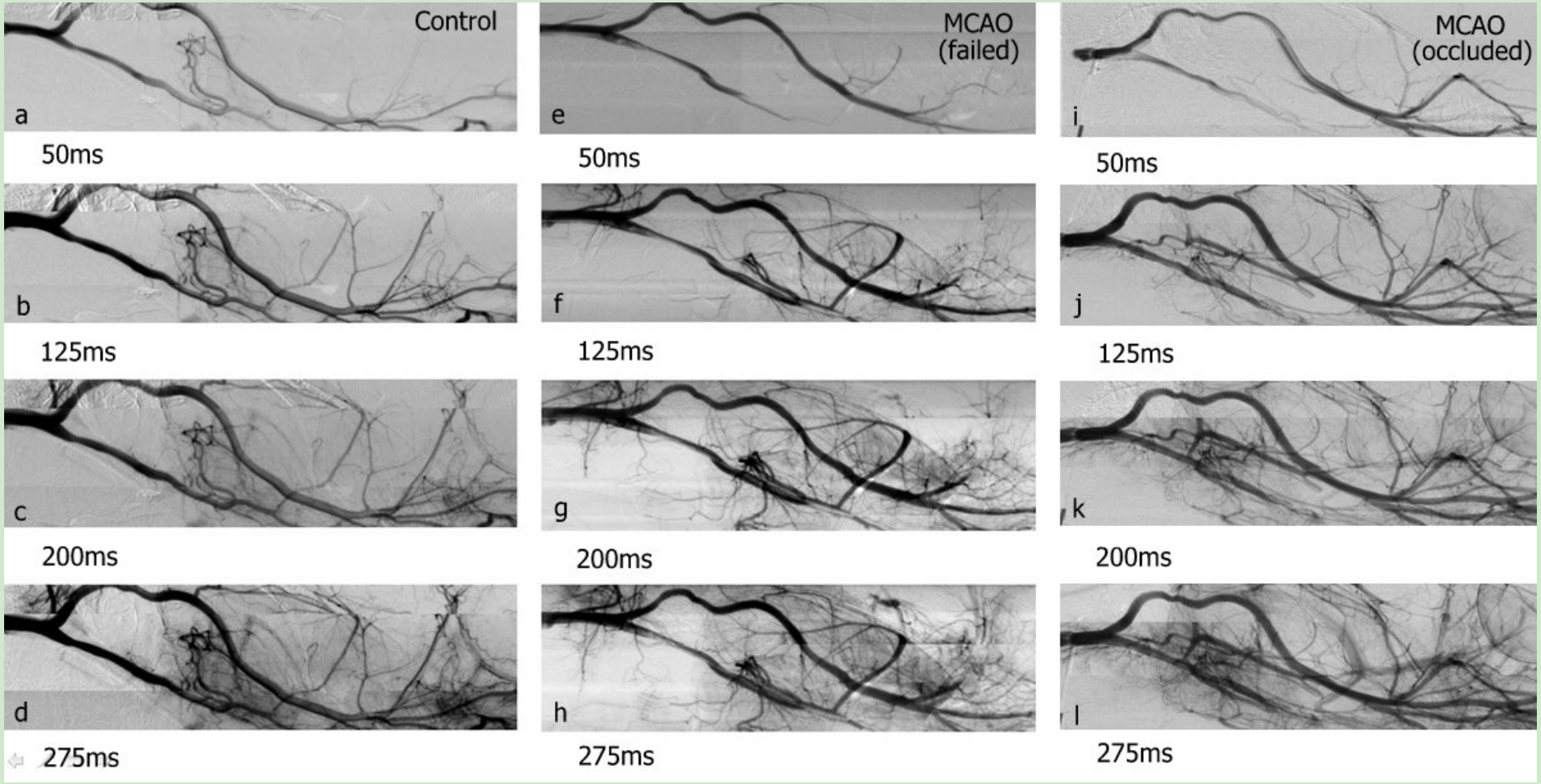

"Effect of Suture Properties on Stability of Middle Cerebral Artery Occlusion Evaluated by Synchrotron Radiation Angiography" Stroke 43, 888, 2012

Yongjing Guan, Yongting Wang, Falei Yuan, Haiyan Lu, Yuqi Ren, Tiqiao Xiao, Kemin Chen, David A. Greenberg, Kunlin Jin and GuoYuan Yang,

Osteogenic evaluation of porous calcium / magnesium scaffold

CS Liu et al.,(East China University of Science and Technology)

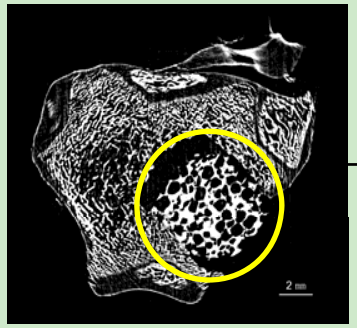

0 Month

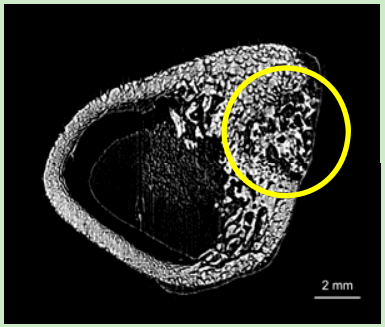

1 Month

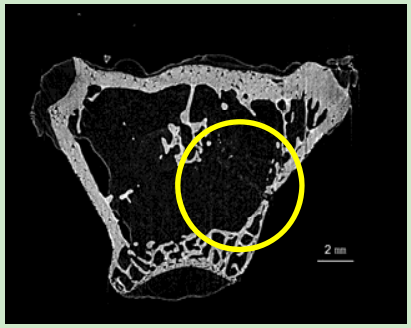

3 Months

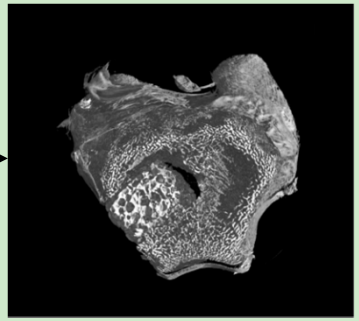

After implanted into rabbit femur cavity defect for 3 months, the porous calcium / magnesium phosphate scaffold completely degraded, and bone defect almost healed. This indicates good biodegradation of the new type of tissue-engineering scaffold.

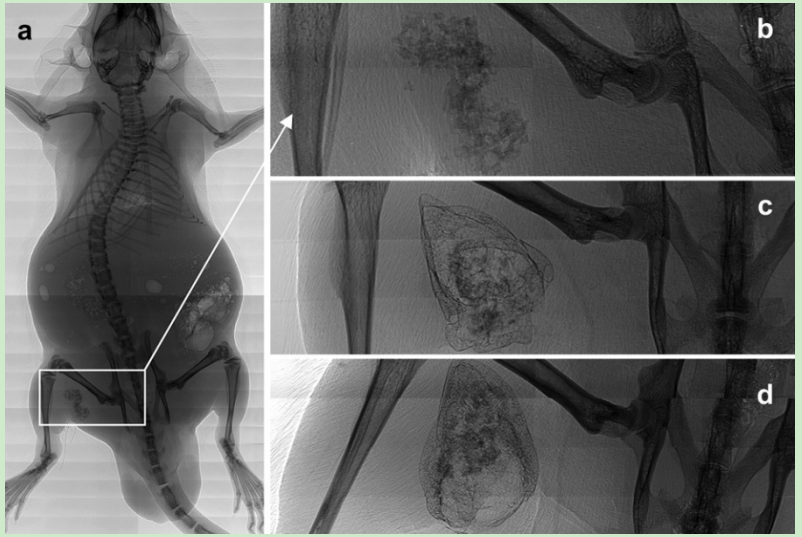

SR X-Ray images of thigh muscle pouches of mice after implantation of scaffolds. (a) CMMS scaffolds without rhBMP-2 at week 4, (b) High-magnification image of (a), (c, d) CMMS/rhBMP-2 scaffolds at week 2 and 4, respectively

Chenglong Dai, Han Guo, Jingxiong Lu, Jianlin Shi, Jie Wei and Changsheng Liu, "**Osteogenic evaluation of calcium/magnesium-doped mesoporous silica scaffold with incorporation of rhBMP-2 by synchrotron radiation-based μCT**"
Biomaterials 32, 8506, 2011

SR-μCT application in ancient eye bead

- **Eye bead** is the article with western Asia style, and it's the evidence of East-West culture communication during the Warring State Period (475BC-221BC)
- Question
  - the eye bead with glassy surface is glass product?
  - There is no scientific evidence of production technology of eye bead.
- SR-μCT has high revolution with relatively bigger field
- Firstly establish nondestructive identification method for faience, glazed pottery and glass
- Testify the production technology of eye bead according to micro analysis

Faience (glazed quartz)

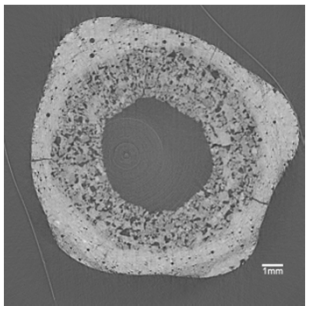

Glazed pottery

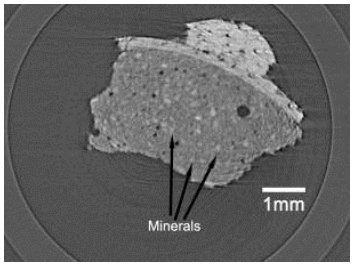

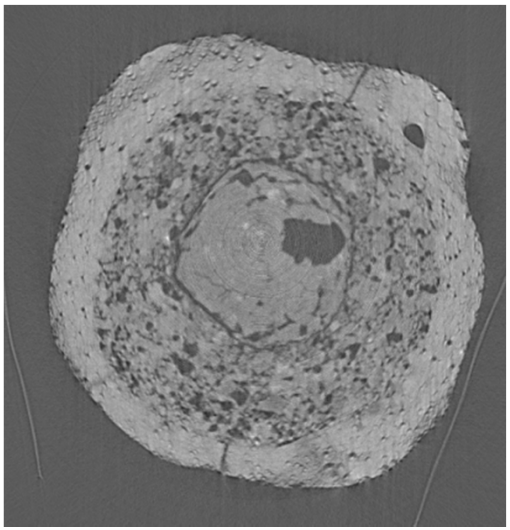

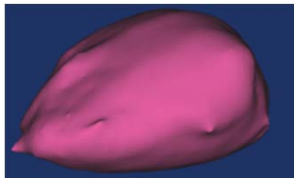

The 3D reconstruction of an oblate air bubble

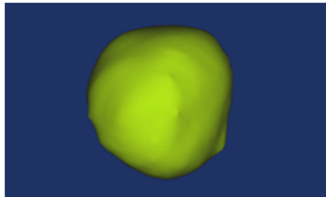

The 3D reconstruction of a spherical air bubble

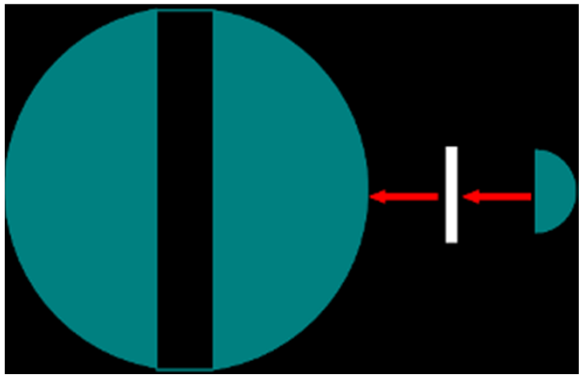

Inlay process

Yimin Yang, Lihua Wang, Shuya Wei, Guoding Song, Jonathan Mark Kenoyer, Tiqiao Xiao, Jian Zhu and Changsui Wang, "**Nondestructive Analysis of Dragonfly Eye Beads from the Warring States Period, Excavated from a Chu Tomb at the Shenmingpu Site, Henan Province, China**"
Microscopy and Microanalysis 19, 335, 2013

New Programs at SSRF

How Many Beamlines at SSRF

➢ 18 Straight sections for IDs

- In vacuum undulators will be employed to produce brilliant X-ray beams and a standard straight section can accommodate two IV-undulators.
- A long straight can accommodate two or more standard undulators
- More than 26 ID beamlines have been scheduled

➢ 20 BMs

Two beamlines can be extracted from each BM at 1° and 3°,
Up to 38 BM ports (including 4 IR ports) available

SSRF has a capacity of accommodating 50~ 60 beamlines

Ongoing projects

◆Five Beamlines for "National Facility for Protein Science"

- Three Protein crystallography beamlines with different fetures
  - Protein micro-crystals: membrane proteins etc.
  - Crystals with large unit cell: macromolecular complexes and assemblies
  - High throughput crystal screening and structural determination
- Small angle X-ray scattering beamline(Bio-SAXS)
  - High performance(very small angle X-ray scattering) beamline for the studies of protein dynamics and interaction
- IR Beamline with two end-stations
  - Time-resolved spectroscopy for protein dynamics and interaction
  - Micro-spectroscopy and imaging for structural and functional studies of cell, tissue and organisms

---- To be completed by December 2013

New Hutches for NFPS Beamlines

Beamline Installation

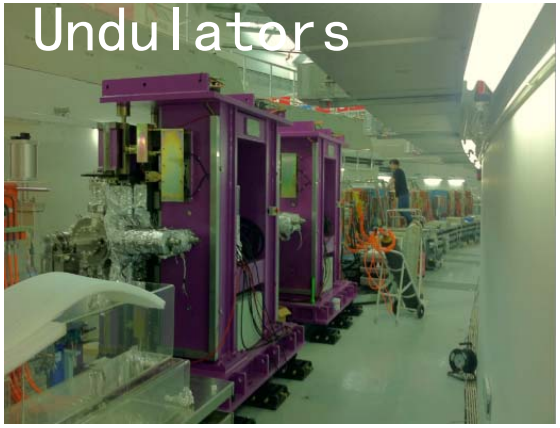

IVU20-1 and IVU20-2

IVU25

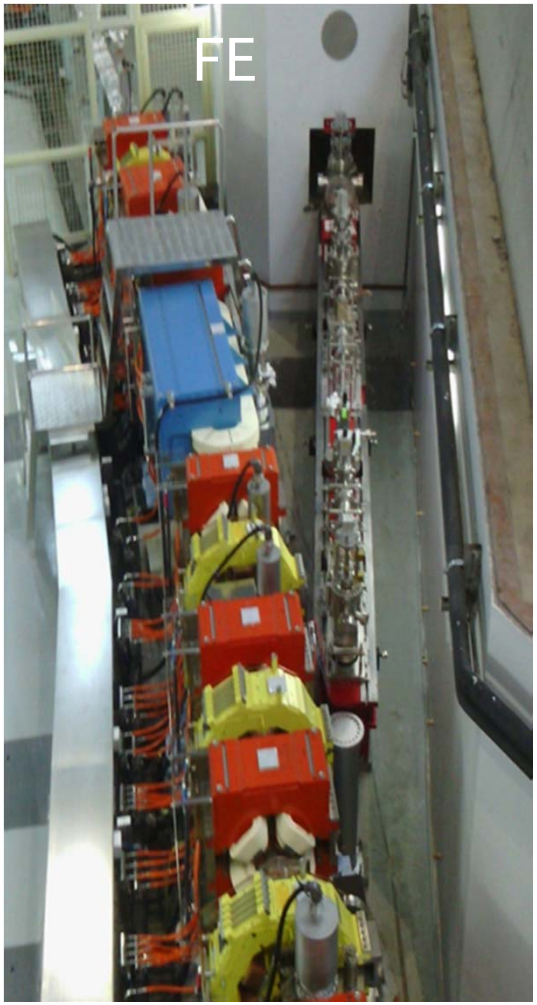

Beamline in commissioning and testing

The End-station of Micro-crystallography Beamline

Micro-Crystallography Beamline (BL18U1) @ SSRF

Experimental goals:

- **Small beam size and high flux**
- **Structural determination of small crystals, 5 ~10 μm**

Design Specifications	
Photon Energy Range:	**5~18 keV**
Energy Resolution:	**≤2×10^{-4} (12keV)**
Focused Beam Size:	**≤10×7 μm (12keV)**
Flux at Sample Position:	**≥5×10^{11} phs/s (12keV,300mA)**
Focused Beam Divergence:	**≤0.7×0.25 mrad^2 (12keV)**
Testing Results	
Photon Energy Range:	**5~18 keV**
Energy Resolution:	**1.8×10^{-4} (12keV)**
Focused Beam Size:	**9.8×5.0 μm (12keV)**
Flux at Sample Position:	**5.8×10^{11} phs/s (12keV,300mA)**
Focused Beam Divergence	**0.27×0.17 mrad^2 (12keV)**

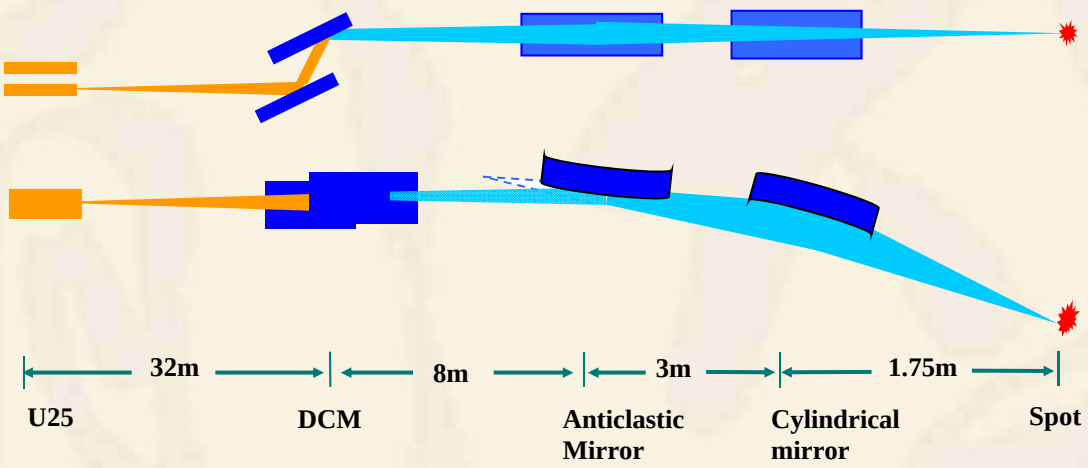

Optical Design of the Beamline

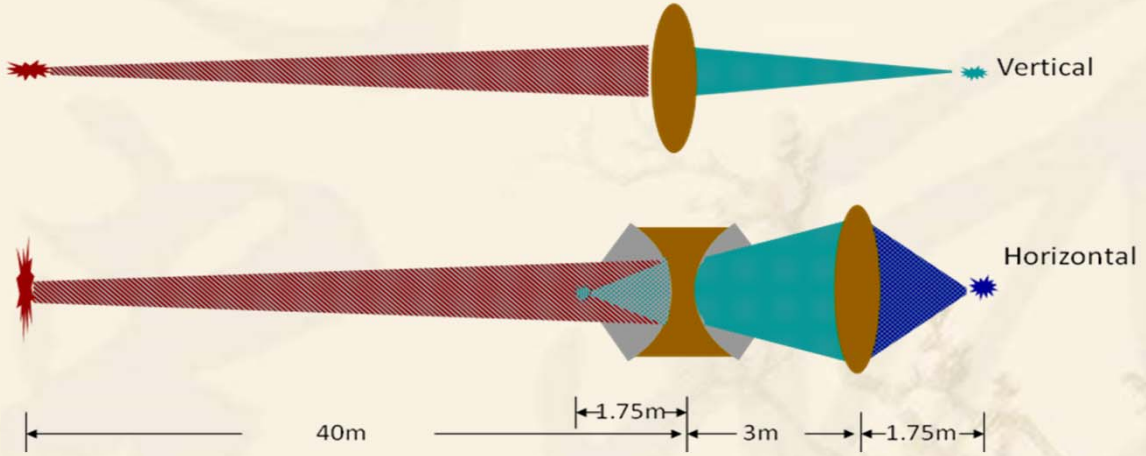

Focusing optics of : anticlastic mirror +cylindric mirror

Features: large and tunable demagnification ratio

BioSAXS Beamline

specifications		
	Design	Test
Photon energy range (keV)	7~15	7~15
Energy resolution	5×10^{-4}	2×10^{-4}
Focus dimension (mm×mm)	0.35×0.11	0.33×0.06
Beam flux (phts/s)	4×10^{12}	5×10^{12}
Beam Divergence (μrad×μrad)	90×30	35×25

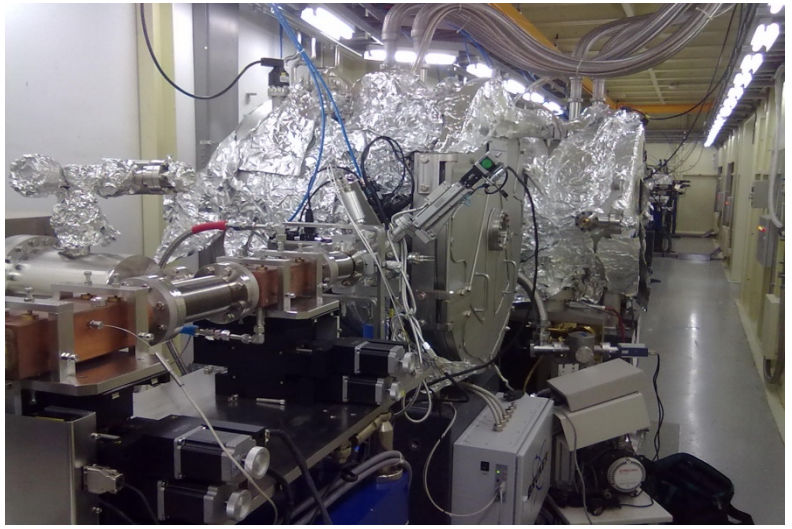

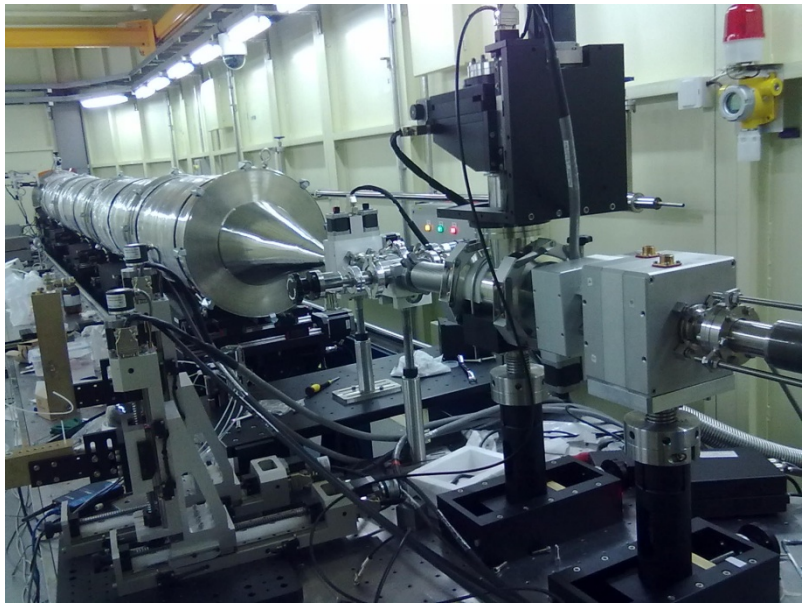

Infrared spectromircoscopy beamline at SSRF (BL01B)

Goals:

Physical phenomenon and biochemical reaction, low frequency vibrational modes and structure dynamics of biological molecule, sub-structure of albumen, spectrum analysis of biologic tissue and structure information of biologic molecule in micro area, spectral imaging of biological cell…

Specifications	Endstation 1	Endstation 2
Techniques	Time resolved infrared spectroscopy	Infrared spectromicroscopy
Source	Edge radiation & Bending magnet	Edge radiation & Bending magnet
Energy range	10 – 100000 cm^{-1}	600 – 100000 cm^{-1}
Spectral resolution	0.1 cm^{-1}	0.2 cm^{-1}
Flux at the sample	>10^{13} (photons/sec/0.1% bw) at 1000 cm^{-1} @300mA	>10^{13} (photons/sec/0.1% bw) at 1000 cm^{-1} @300mA
Time resolution / Focused beam size	10 ns with step-scan mode	<30 μm @ 1000 cm^{-1}

All specifications are available.

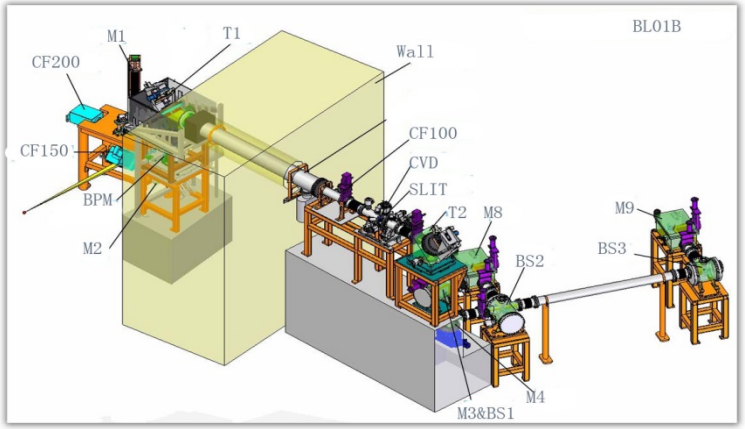

- ❑The IR radiation is collected (-10~10 mrad in vert. and -15~25 mrad in horiz.) by the extraction mirror M1 at 1815 mm from the source.
- ❑ The water-cooled M1 mirror has a central slot of 2.6mm to avoid overheating by the X-ray beam.
- ❑ The wedged CVD diamond window separates the UHV of the storage ring and the rough vacuum of the IR beamline.
- ❑ The toroidal mirror T2 provides collimated beam.
- ❑FTIR spectrometer and IR microscope are equiped in the endstations.

Absolute Flux Measurement

Measured Flux @1um Before FTIR	Endstation I Time resolved infrared spectroscopy	Endstation II Infrared spectromicroscopy
	1.3×10^{13} (photons/sec/0.1% b.w.)	1.9×10^{13} (photons/sec/0.1% b.w.)

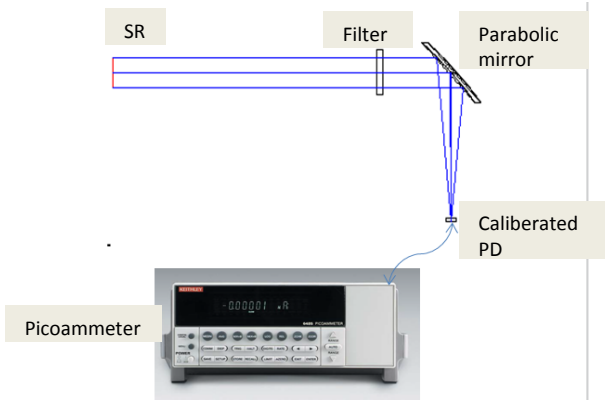

Focused Beam Profile

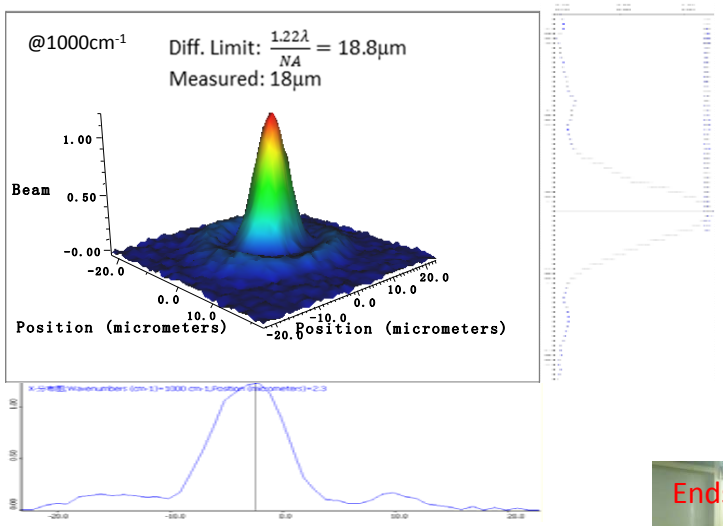

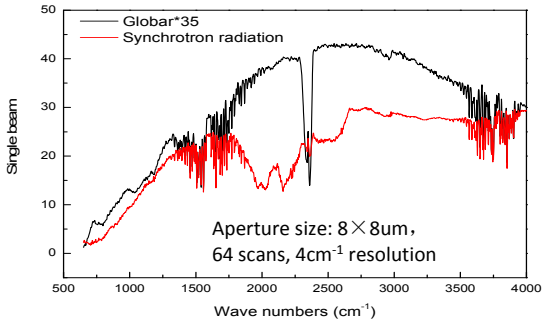

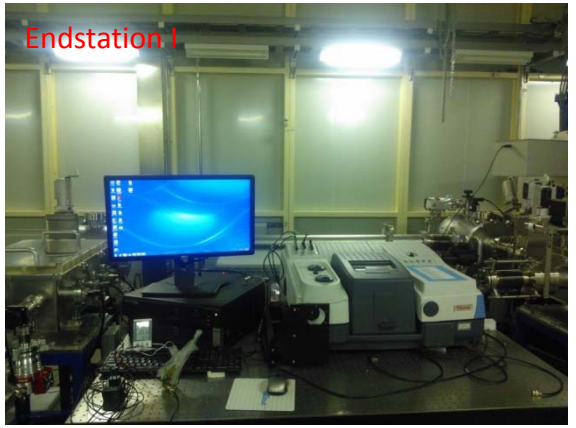

One Soft X-ray Beamline with Extremely High Resolultion for ARPES and PEEM :

Dreamline

ARPES + PEEM

high spatial resolution (<10 nm)

High energy resolution (2 meV@20 eV, 10 meV@1000 eV)
Low temperature （<1 K)
Dual EPU, 20-2000eV

- **Proposed by Insitute of Physics, CAS:**

Construction started in 2010 and to be completed soon

Construction of Dreamline

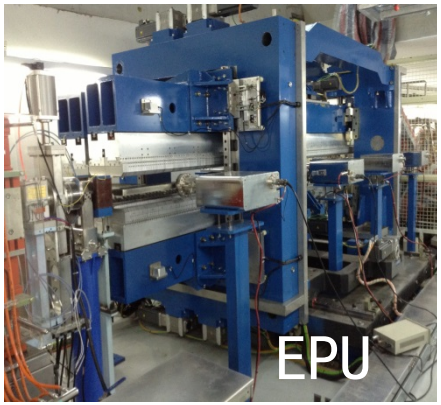

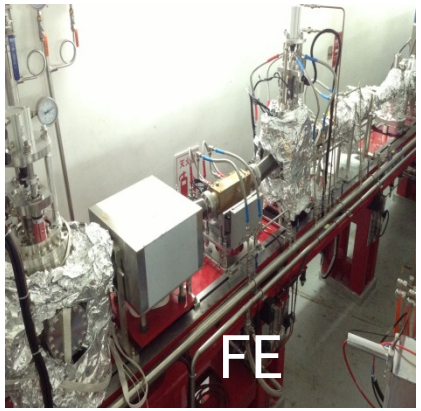

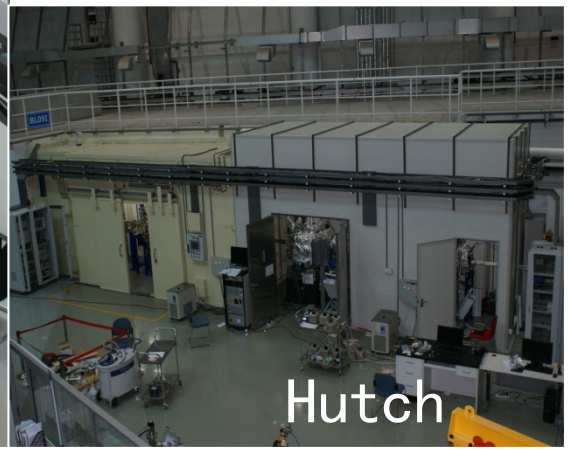

Other Beamlines under Construction

- SiP.ME^2 Project (2013- 2017)
  - Angle resolved photon electron spectroscopy (EPU, 10-100eV)
  - Ambient pressure photon electron spectroscopy (BM, 40-2000eV)

Future Programs

◆ SSRF Phase II project: in the proposal

- 16 public beamlines have been proposed as the preliminary program, by making full use of the brilliant beam to achieve:
  - high spatial resolution: ~10nm
  - high energy resolution: ~1mev
  - fast time resolution: ~100ps

  To facilitate the research in broad fields.

◆ Industrial Bemalines

SinoPEC plans to build three beamlines for their specific use.

Proposed SSRF Phase-II Beamlines (16)

Disciplines	Beamline	Science goals
Energy science	E-line	Energy conversion and control
	D-Line	Structure of non-equilibrium systems
	Radioactive materials	Radioactive material
	Hard X-Ray S…	
Environmental Science	Hard …	…onents
	…	
	…	
Materials Science	…	
	…	
	…	
	…	
Life Science	P…	
	Membr…	
Industry Applications	Ultra Hard X-ray App…	…ials and rocks
	Time-resolved USAXS	self-assembly and fiber-spinning
	Fast X-ray imaging	Fast process imaging

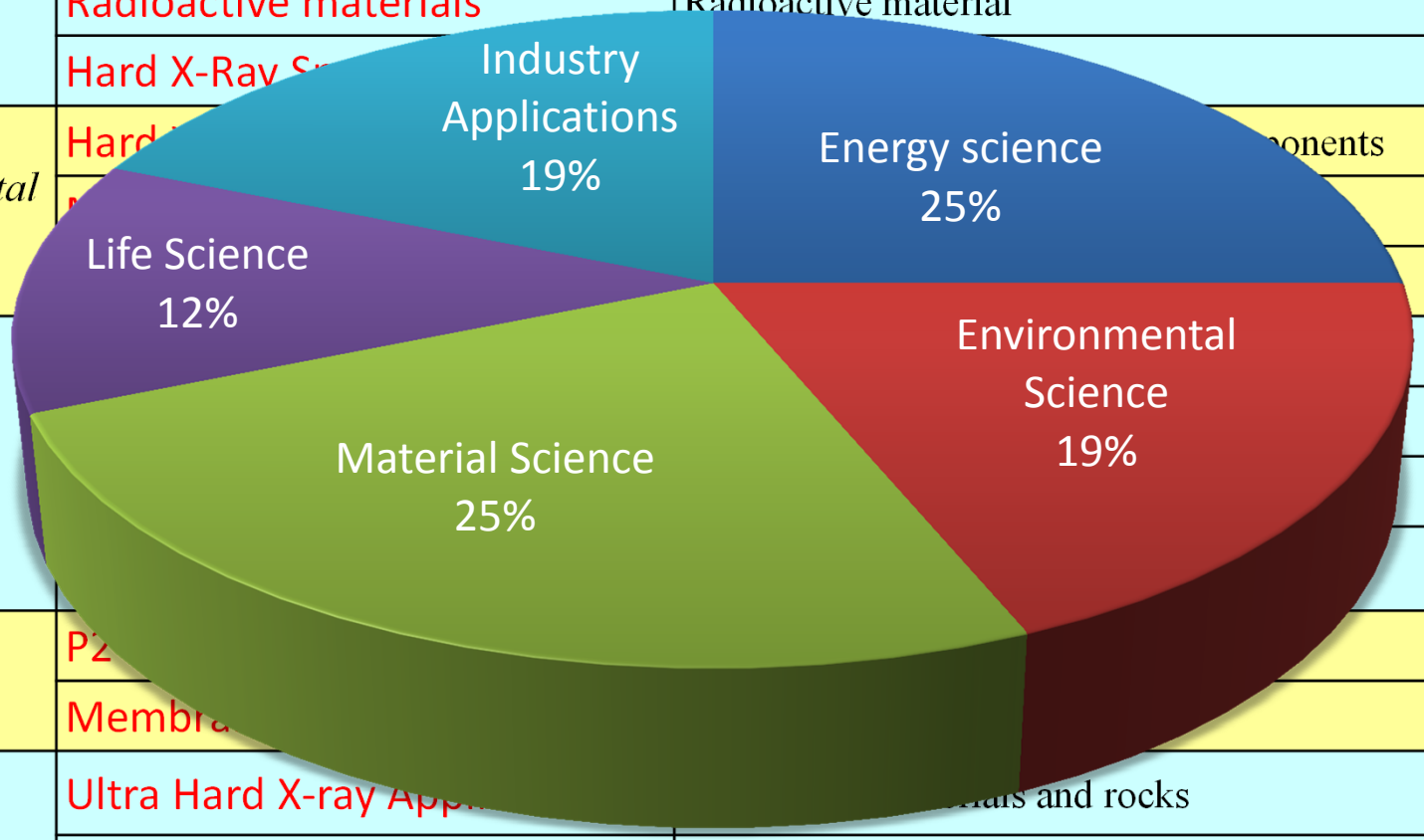

Beamlines at SSRF By 2020

- 7 Phase I beamlines
- 8 Bea
- 1
-

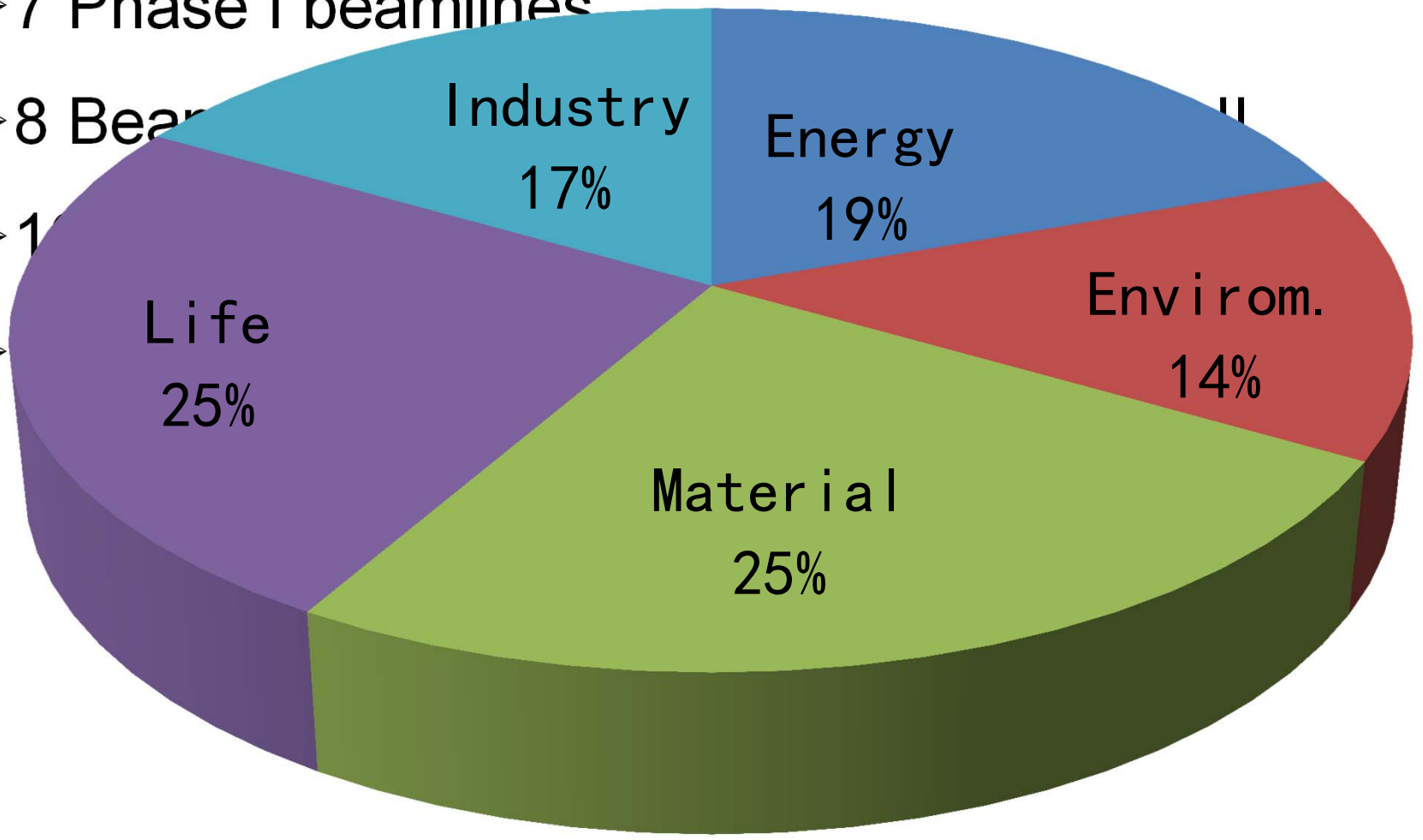

Shanghai Soft X-ray Free Electron Laser project

SXFEL is a test facility for performing the "proof of principle" of the cascading HGHG, cascaded EEHG-HGHG and prototyping the key FEL technologies toward the HGHG based XFEL;

SXFEL parameters

Parameters	Design value
Electron Energy	**0.84 GeV**
Normalized emittance	< 2.5mm.mrad
Slice energy spread	< 0.02%
Peak current/ bunch length/ charge	500 A /1ps/ 500pC
Wavelength of laser seed	~265nm
Scheme	HGHG,
Cascading scheme	265-44-9nm;
Modulator undulator	Tunable gap, hybrid planar
Radiator undulator	Hybrid planar
FEL peak power	>100MW
FEL wavelength	**9 nm**
FEL pulse length	100~150 fs (FWHM)

The construction of SXFEL has been approved and it will begin soon

SXFEL main building

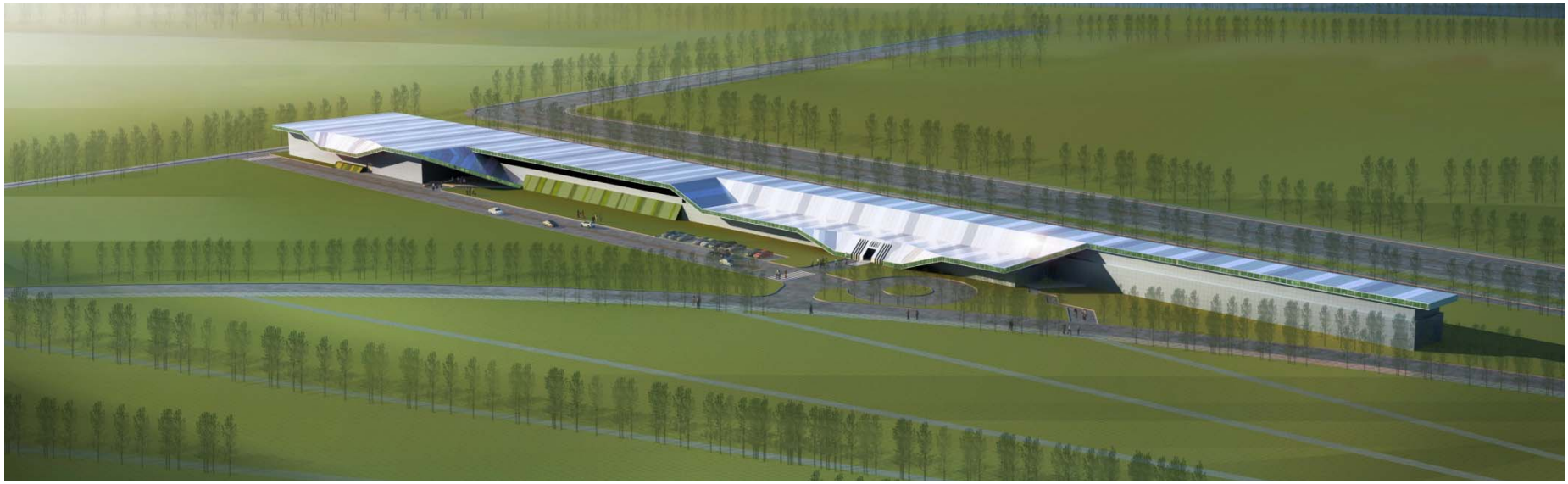

Building area: 5500 m²

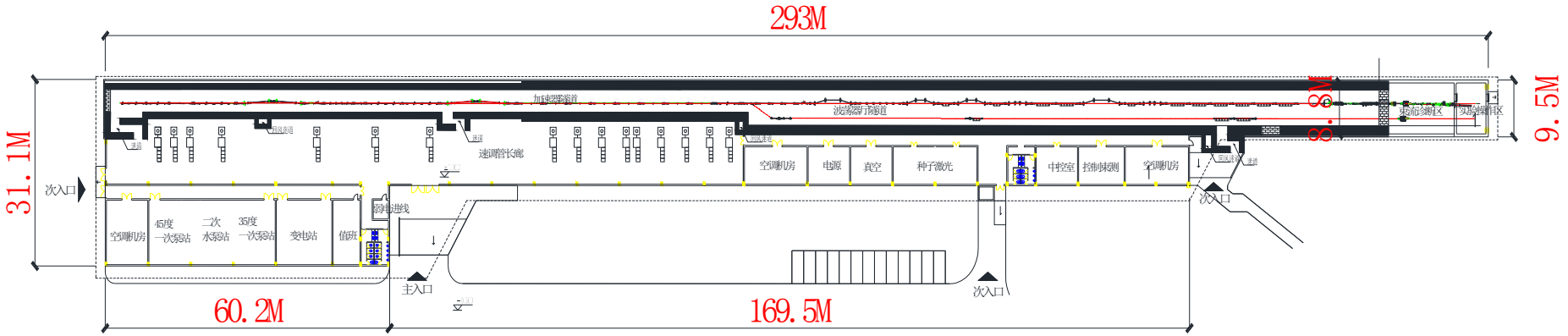

Shanghai Center for Photon Science

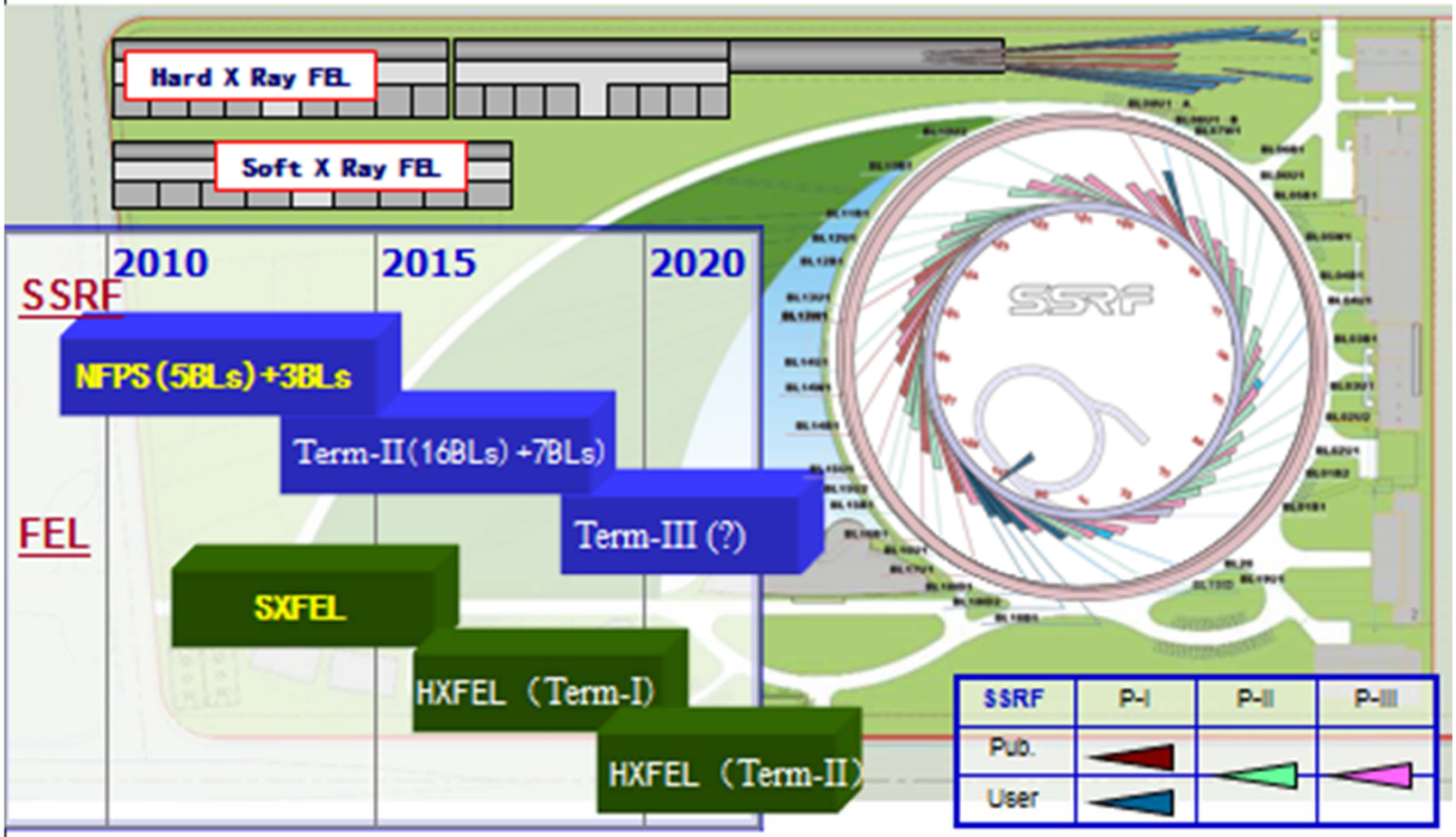

To become a world-class photon science center

Thank you for your attention!